AGU PUBLICATIONS

Journal of Advances in Modeling Earth Systems

RESEARCH ARTICLE

10.1002/2015MS000607

Key Points:
- Seven clusters are identified from the historical and predicted TC tracks for the period 1980–2013
- The prediction of WNP TC frequency shows skill higher than FLOR-FA in most of initialization months
- The prediction of TC landfall with hybrid models outperforms FLOR-FA for all initialization months

Supporting Information:
- Supporting Information S1

Correspondence to:
W. Zhang,
wei.zhang@noaa.gov

Citation:
Zhang, W., G. Villarini, G. A. Vecchi, H. Murakami, and R. Gudgel (2016), Statistical-dynamical seasonal forecast of western North Pacific and East Asia landfalling tropical cyclones using the high-resolution GFDL FLOR coupled model, *J. Adv. Model. Earth Syst.*, *8*, 538–565, doi:10.1002/2015MS000607.

Received 10 DEC 2015
Accepted 27 MAR 2016
Accepted article online 31 MAR 2016
Published online 15 APR 2016

Statistical-dynamical seasonal forecast of western North Pacific and East Asia landfalling tropical cyclones using the high-resolution GFDL FLOR coupled model

Wei Zhang[1,2,3], Gabriele Villarini[4], Gabriel A. Vecchi[1,2], Hiroyuki Murakami[1,2], and Richard Gudgel[1]

[1]National Oceanic and Atmospheric Administration/Geophysical Fluid Dynamics Laboratory, Princeton, New Jersey, USA, [2]Atmospheric and Oceanic Sciences Program, Princeton University, Princeton, New Jersey, USA, [3]Key Laboratory of Meteorological Disaster, Ministry of Education, Nanjing University of Information Science and Technology, Nanjing, China, [4]IIHR-Hydroscience and Engineering, University of Iowa, Iowa City, Iowa, USA

Abstract This study examines the seasonal prediction of western North Pacific [WNP] and East Asia landfalling tropical cyclones (TCs) using the Geophysical Fluid Dynamics Laboratory(GFDL) Forecast-oriented Low Ocean Resolution version of CM2.5 with Flux Adjustment (FLOR-FA) and finite-mixture-model (FMM)-based statistical cluster analysis. Using the FMM-based cluster analysis, seven clusters are identified from the historical and FLOR-FA-predicted TC tracks for the period 1980–2013. FLOR-FA has significant skill in predicting year-to-year variations in the frequency of TCs within clusters 1 (recurving TCs) and 5 (straight-moving TCs). By building Poisson regression models for each cluster using key predictors (i.e., sea surface temperature, 500 hPa geopotential height, and zonal vertical wind shear), the predictive skill for almost all the clusters at all initialization months improves with respect to the dynamic prediction. The prediction of total WNP TC frequency made by combining hybrid predictions for each of the seven clusters in the hybrid model shows skill higher than what achieved using the TC frequency directly from FLOR-FA initialized from March to July. However, the hybrid predictions for total WNP TC frequency initialized from January to February exhibit lower skill than FLOR-FA. The prediction of TC landfall over East Asia made by combining the hybrid models of TC frequency in each cluster and its landfall rate over East Asia also outperforms FLOR-FA for all initialization months January through July.

1. Introduction

Tropical cyclones (TCs) cause severe hazards and numerous fatalities to coastal and inland regions [e.g., *Pielke*, 1997; *Pielke et al*., 2008; *Zhang et al*., 2009]. The vast majority of the damage caused by TCs occurs during or after landfall [e.g., *Landsea et al*., 1998; *Powell and Houston*, 1998]. An accurate and timely seasonal forecasting of TC activity (e.g., frequency and landfall) is thus of great importance to both scientific communities and governmental administration.

Over the recent decades, considerable attention has been paid to improve TC predictions based on statistical methods and dynamic models [e.g., *Nicholls*, 1979; *Gray et al*., 1993; *Marks and Shay*, 1998; *Chan et al*., 2001; *Fan and Wang*, 2009; *Vecchi et al*., 2010, 2013, 2014; *Villarini and Vecchi*, 2013]. Statistical models have been used to forecast TC occurrence frequency/genesis [e.g., *Chan*, 1995; *Chan et al*., 1998, 2001; *Klotzbach*, 2007; *Wang et al*., 2013; *Zhang et al*., 2015], track [e.g., *J.-H. Kim et al*., 2012; *Zhang et al*., 2013a], landfall [e.g., *Goh and Chan*, 2010; *Zhang et al*., 2013a,2013b], and intensity [e.g., *Knaff et al*., 2005; *Zhang et al*., 2013d] in the western North Pacific (WNP). Scientists have widely used Poisson regression [e.g., *Liu and Chan*, 2003; *Chu and Zhao*, 2007], Bayesian models [e.g., *Chu et al*., 2010; *Lu et al*., 2010], and multiple linear regression models [*Fan*, 2007; *Fan and Wang*, 2009] to predict the occurrence and frequency of WNP TCs.

To complement statistical models, state-of-the-art climate models, including atmospheric general circulation models (AGCMs) and coupled GCMs (CGCMs) have shown encouraging skill in seasonal forecasting of TC frequency [e.g., *Vitart et al*., 2007; *Smith et al*., 2010; *Zhao et al*., 2010; *Chen and Lin*, 2011; *Vecchi et al*., 2014; *Camp et al*., 2015], and landfall over East Asia [e.g., *Sun and Ahn*, 2011; *Au-Yeung and Chan*, 2012; *Huang and Chan*, 2014; *Tan et al*., 2015]. Over the years, hybrid models combining dynamic and statistical models, have proven highly skillful in the prediction of TCs in the North Atlantic and the WNP [e.g.,

Klotzbach, 2007; *Elsner et al*., 2008; *Vecchi et al*., 2010; *LaRow*, 2013; *Villarini and Vecchi*, 2013; *Li et al*., 2013; *Vecchi et al*., 2013, 2014; *Kim et al*., 2014]. *Huang and Chan* [2012] reported that the dynamically downscaled forecasts of TC landfall over East Asia outperform the original CFS2 prediction with a correlation of 0.27 and a RMSE of 3.72, while that for TC frequency is 0.55 with a leave-one-out cross-validation. *Sun and Ahn* [2011] reported that the coupled climate model (PNU-CGCM) exhibited virtually no forecasting ability in predicting 6–9 month and 3–5-month leads for landfalling TCs over East Asia. Based on statistical relationships between TC frequency/landfall and physical processes tied to dynamical models, the so-called hybrid dynamical-statistical models have been capable of predicting seasonal TC activity over the North Atlantic and the WNP [e.g., *Wang et al*., 2009; *Kim and Webster*, 2010; *Vecchi et al*., 2010; *Sun and Chen*, 2011; *Li et al*., 2013; *Villarini and Vecchi*, 2013; *Vecchi et al*., 2013; *Kim et al*., 2014; *Vecchi and Villarini et al*., 2014]. Hybrid models take advantage of both statistical associations derived from the observations and dynamic models, and environmental variables simulated by dynamic models to improve the skill of the prediction.

Cluster analysis is a useful method to group data based on some metrics (e.g., distance or similarity) and has been widely applied to unravel inherent and relevant patterns from historical TC data [e.g., *Camargo et al*., 2007a,2007b; *Gaffney et al*., 2007; *Ramsay et al*., 2011]. Seven clusters have been identified from the historical TC tracks in the WNP [*Camargo et al*., 2007a,2007b; *H.-S. Kim et al*., 2012]. TCs from the same cluster share similarity in moving direction, genesis, track shape, and landfall regions [*Camargo et al*., 2007a,2007b; *Kim et al*., 2010]. If every single TC cluster is predictable, the basin total TC activity should also be predictable. *H.-S. Kim et al*. [2012] applied the results of cluster analysis to predict seasonal TC track density in the WNP and showed encouraging performance. *Choi et al*. [2016] have used cluster analysis results to predict the frequency of intense tropical cyclones in the WNP and North Atlantic. It is thus of broad scientific and societal interest to examine whether we can improve seasonal predictions of WNP TC frequency and East Asia landfall frequency by integrating the cluster analysis of TC tracks. The basic hypothesis is that the development of prediction models for each cluster may lead to more skillful forecasts than what could be attained by developing a single model that would have to work on all the clusters combined.

The Geophysical Fluid Dynamics Laboratory (GFDL) Forecast-oriented Low Ocean Resolution Version of CM2.5 with Flux Adjustment (FLOR-FA) has been providing seasonal forecasts for regional hurricane activity in the North Atlantic, midlatitude storm tracks and surface air temperature [*Vecchi et al*., 2014; *Jia et al*., 2015; *Yang et al*., 2015]. Although FLOR-FA has some biases in predicting TC density in the WNP [*Vecchi et al*., 2014], the prediction of TC frequency or landfall might be further improved by developing a hybrid model integrating statistical relationships between observations and simulations. *Murakami et al*. [2016] applied a hybrid model to predict North Atlantic TCs and showed that the hybrid model improves basin-total and U.S. landfalling TC frequency. Therefore, given the promising results for the North Atlantic, it is of significant interest to build a hybrid model for seasonal predictions of total WNP TC frequency and landfall over East Asia, where most of wealth and people are accumulated along the coastal regions.

The objectives of this study are thus: (i) to assess the predictability of TC frequency and landfall over East Asia with FLOR-FA; (ii) to unravel clusters from historical and simulated TC tracks using cluster analysis; and (iii) to improve seasonal predictions of total WNP TC frequency and landfall over East Asia using a combination of statistical methods and dynamic models. This study would advance our understanding of TC activity and landfall over East Asia, providing basic information that could lead to an improved preparedness, management and mitigation of TC-related hazards in Asia.

The remainder of this paper is organized as follows. Section 2 presents the data and methodology, followed by a description of the results of the analyses. Section 4 summarizes the main points and concludes the paper.

2. Data and Methodology

2.1. Data

TC data are obtained from International Best Track Archive for Climate Stewardship (IBTrACS) [*Knapp et al*., 2010] for the period of 1980–2013. Monthly estimates of sea surface temperature (SST) are taken from the Met Office Hadley Centre HadSST3.1.1.0 [*Kennedy et al*., 2011]. Following previous studies [*Wu et al*., 2004; *Zhang et al*., 2012], we consider as landfalling TC over East Asia a storm that makes landfall over the East Asian coast shown in Figure 1.

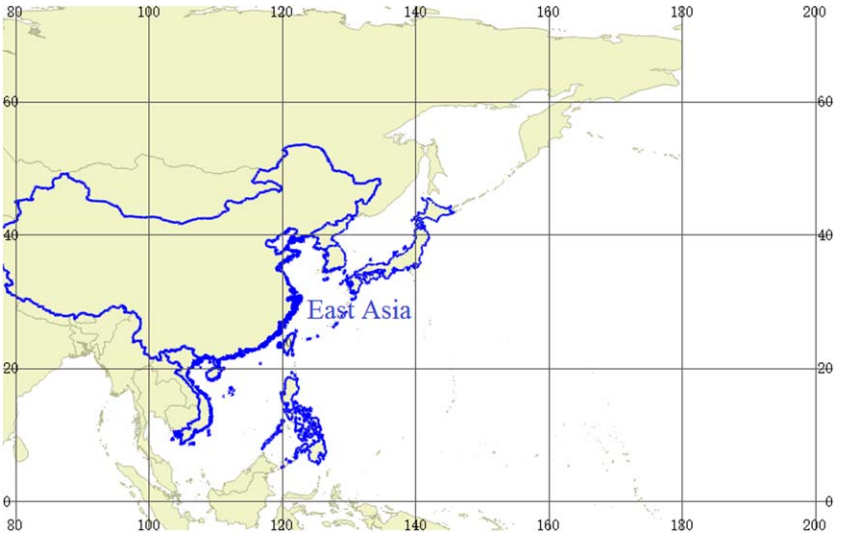

Figure 1. The East Asian coast (blue) which is used to define TC landfalls over East Asia.

2.2. Dynamic Model

We use a state-of-the-art high-resolution coupled climate model, the Forecast-oriented Low Ocean Resolution (FLOR) configuration of GFDL's Coupled Model version 2.5 (CM2.5) [*Delworth et al*. 2012]. FLOR is built by a combination of oceanic and ice components derived from GFDL Coupled Model version 2.1 (CM2.1) [*Delworth et al*., 2006], and the atmosphere and land components of CM2.5 [*Delworth et al*., 2012]. The atmosphere and land models are identical to those in CM2.5, and have a spatial resolution of approximately 50 km × 50 km [*Delworth et al*. 2012]. The ocean model of CM2.5 has a 0.25° × 0.25° spatial resolution [*Delworth et al*. 2012] while the ocean and sea ice components of FLOR are directly taken from CM2.1 at 1° × 1° spatial resolution, with the exception of a refinement of the grid in the deep tropics (from 10°S to 10°N) to approximately 1/3° in meridional direction. CM2.1 has been widely used for climate research, predictions and projections for around a decade. The ocean component of FLOR has been slightly changed compared with CM2.1 by incorporating a newer and higher order advection scheme, a parameterization for eddies [*Farneti et al*., 2010] and a more realistic representation of the solar absorption by the ocean and a biharmonic horizontal viscosity scheme. Most of the computing expenses with FLOR are spent in the atmosphere and land components. A detailed description of the FLOR model is documented in *Vecchi et al*. [2014] and references therein.

We use here a version of FLOR in which the model's momentum, enthalpy and freshwater fluxes from atmosphere to ocean are adjusted to bring the model's long-term climatology of SST and surface wind stress closer to observations—this is known as the "flux adjusted" version of FLOR, or FLOR-FA [*Vecchi et al*. 2014; *Delworth et al*., 2015; *Yang et al*., 2015]. Previous studies have demonstrated more realistic simulation of TC genesis and density in the North Atlantic and the WNP with FLOR-FA than FLOR [e.g., *Vecchi et al*. 2014; *Krishnamurthy et al*. 2016].

The seasonal predictions are initialized using the GFDL's ensemble coupled data assimilation (ECDA) system, which utilizes an ensemble-based filtering algorithm to the CM2.1 (for more details on ECDA, consult *Zhang et al*. [2007] and *Zhang and Rosati* [2010]). The ECDA covers the period from 1960 to the present and is being updated monthly for GFDL's seasonal-to-decadal experimental forecasts [*Yang et al*., 2012, 2015; *Vecchi et al*., 2011, 2013, 2014; *Jia et al*., 2014; *Msadek et al*., 2014a,2014b]. A comprehensive assessment of the 1960–2010 oceanic variability in the latest version of the ECDA can be found in *Chang et al*. [2013]. It should be noted that the initial conditions of different components of FLOR are taken from different available sources at GFDL because the data assimilation system for FLOR is still under development [*Vecchi et al*. 2014]. The initial conditions for the ocean and ice components of the FLOR hindcasts are from the ECDA, whereas the initial conditions for the atmosphere and land components are taken from FLOR atmosphere-only simulations with prescribed observed SSTs [*Vecchi et al*. 2014]. The 12 member ensemble seasonal hindcasts are initialized on the 1st day of every month from 1980 to 2014 and integrated for 12 months

with temporally varying anthropogenic and natural forcing [*Vecchi et al*. 2014]. The seasonal hindcast anomalies for each variable were obtained by subtracting the lead-time-dependent climatology from the hindcasts.

2.3. Cluster Analysis Method

We use finite-mixture-model (FMM)-based cluster analysis to group TC tracks from both observations and 12 ensemble seasonal forecasting experiments. This method has been widely applied to TC tracks in various ocean basins [*Camargo et al*., 2007a,2007b,2008; *Zhang et al*., 2013c] and it provides a rigorous probabilistic framework to cluster TC tracks of various shapes and lengths. This algorithm employs mixed polynomial regression models (i.e., curves) to fit the geographical "shape" of TC tracks and model a TC's longitudinal and latitudinal positions versus time [*Gaffney and Smyth*, 1999; *Gaffney*, 2004; *Camargo et al*., 2007a,2007b; *Zhang et al*., 2013c].Assuming that there are K clusters in the TC tracks represented by K different regression models, each TC track is represented by one of K different regression models with its own shape parameters. The primary objectives of such modeling strategy are to estimate and learn the parameters of all K models from TC tracks, and to infer to which of the K regression models each TC track most likely belongs. Given the FMM, each TC track is assigned to the mixture component (i.e., the cluster) that most probably generates the track and the assigned cluster of the TC track has the highest posterior probability. The Expectation Maximization (EM) algorithm is used to estimate these model parameters [*McLachlan and Krishnan*, 1997].

The details of the FMM-based cluster analysis are described as follows. Assuming that $p(x;\theta)$ is a d-dimensional probability density function depending on a multidimensional parameter vector θ and $S(\theta)$ an multidimensional cumulative distribution function [*Camargo et al*., 2007a,2007b]. Then

$$f(x)=\int p(x;\theta)dS(\theta) \tag{1}$$

where $S(\theta)$ is the mixing distribution; $S_i(\theta_i)$ is discrete and probability is assigned to only a finite number of points (θ_i; i=1, . . .,k). The finite mixture model can be calculated by summing up all the discrete points to replace the integral in equation (1):

$$f(x)=\sum_{i=1}^{c} S_i(\theta_i)\cdot p(x;\theta_i), \tag{2}$$

In this study, the model is constructed following *Camargo et al*. [2007a,2007b]

$$y_i=T_i\beta+\varepsilon_i,\ \varepsilon_i\sim\mathcal{N}\left(0,\sum\nolimits_k\right), \tag{3}$$

$$P(y_i\mid T_i)=\mathcal{N}\left(T_i\beta,\ \sum\nolimits_k\right), \tag{4}$$

where

$$T_i=\begin{pmatrix}1 & \cdots & x_{i1}^{p}\\ \vdots & \ddots & \vdots\\ 1 & \cdots & x_{in}^{p}\end{pmatrix}, \tag{5}$$

is the regression matrix with an n×p dimension; $\mathcal{N}$ denotes normal distribution; β represents the regression coefficients, y_i is the *i*th TC track having n spatial points (i.e., observations with latitude and longitude), ε_i denotes an $n_i\times 2$ matrix of multivariate Gaussian noise with zero mean and 2×2 covariance matrix $\sum_k$with the diagonal elements $\sigma_{k1}^2$and σ_{k2}^2.

The conditional probability density for the *i*th TC track on the membership of the kth cluster, is defined as

$$p(y_i|T_i,\theta_k)=f\left(y_i|T_i\beta_k,\sum\nolimits_k\right)=(2\pi)^{-n_i}\left|\sum\nolimits_k\right|^{-n_i/2}\exp\left\{-\frac{1}{2}tr\left[(y_i-T_i\beta_k)\sum_k^{-1}(y_i-T_i\beta_k)\right]'\right\}, \tag{6}$$

where $\theta_k=\left(\beta_k,\ \sum\nolimits_k\right)$, and *tr* denotes the trace of a matrix.

We can obtain the regression mixture model with K clusters

$$p(y_i|T_i,\ \phi)=\sum_k^K \alpha_k p_k(y_i|T_i,\theta_k)=\sum_k^K \alpha_k f_k\left(y_i|T_i\beta_k,\sum\nolimits_k\right), \tag{7}$$

where α_k denotes the proportion of a TC track belonging to the kth cluster with the constraint that $\sum_k \alpha_k=1$ and ϕ represents the set of mixture parameters $(\alpha_k,\ \beta_k,$ and $\sum_k)$.

If the complete set of n TC tracks are denoted as $Y=[y_1, \ldots, y_n]$ and the set of measurement times as $T=[t_1, \ldots, t_n]$, the full probability density of Y given T is shown as:

$$p(Y|T,\phi)=\prod_i^n \sum_k^K \alpha_k f_k\left(y_i|T_i\beta_k,\sum\nolimits_k\right). \tag{8}$$

The estimation of the parameters for the model are obtained by maximizing likelihood method. One of the K models with which each TC track is most probably associated can be inferred as soon as the model is properly trained.

The EM algorithm finds the local maximum likelihood through iterative estimations. The E-step and M-step form the EM algorithm. In E-step, we calculate the membership probability that TC track i belongs to cluster k as follows:

$$w_{ik}=\frac{\alpha_k f_k\left(y_i|T_i\beta_k,\sum_k\right)}{\sum_j^K \alpha_j f_j\left(y_i|T_i\beta_j,\sum_j\right)}. \tag{9}$$

Note that w_{ik} denotes the ratio of the likelihood of the ith TC trajectory under the kth cluster to the total likelihood of the ith TC track under all clusters. The $w_{ik}=w_{ik}\mathbf{I}_{n_i}$, where $\mathbf{I}_{n_i}$ is an n_i vector of ones. $W_k=\mathrm{diag}(w'_{1k},\ldots,w'_{nk})$ represents an N × N diagonal matrix. In the M-step, W_k is used to calculate the mixture parameters. The calculating process is similar to the weighted least squares commonly used in regression analysis. The estimated parameters are

$$\begin{aligned}\hat{\beta}_k&=\left(X'W_kX\right)^{-1}X'W_kY,\\ \hat{\sum}_k&=\frac{\left(Y-X\hat{\beta}_k\right)'W_k\left(Y-X\hat{\beta}_k\right)}{\sum_i^n w_{ik}},\\ \hat{\alpha}_k&=\frac{1}{n}\sum_i^n w_{ik}.\end{aligned} \tag{10}$$

The EM algorithm performs iteratively the E and M steps until convergence, which is reached when the ratio of the incremental improvement in log-likelihood to the initial incremental improvement during the second iteration drops below a certain threshold (e.g., 1×10^{-6}). The EM algorithm randomly chooses a set of membership weights W_k and implement the M step. We use the solution with the highest likelihood obtained from 100 starts of the EM algorithm.

2.4. Poisson Regression Model

Poisson regression model has been widely used to analyze the probability for the occurrence of rare events [e.g., hurricanes, tornados, and epidemics; e.g., *Elsner and Schmertmann*, 1993; *Elsner and Jagger*, 2006; *Villarini et al*., 2010; *Wilks*, 2011].

$$P(Y_i=y)=\frac{\mu_i^y e^{-\mu_i}}{y!},\ y=0,\ 1,\ 2\ \ldots\infty \tag{11}$$

where $\log\ (\mu_i)=\beta_0+\sum_j \beta_j x_{ij}$.

If Y follows a Poisson distribution, the logarithm of the expected number of landfalling/WNP TC occurrence μ_i, can be modeled as a linear combination of the predictors x_{ij}, with j being the specified predictor during the year i; β_j is the corresponding Poisson regression coefficient, β_0 the intercept, and y the observed count of

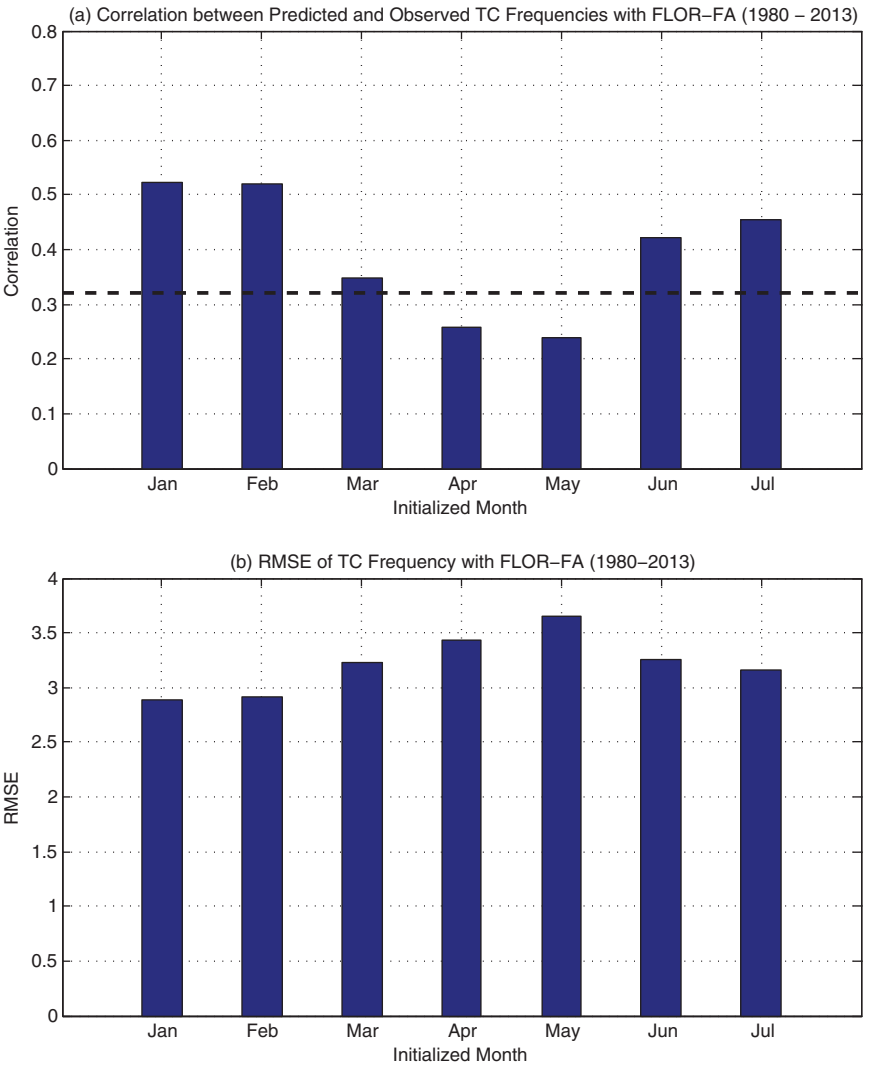

Figure 2. (top) The correlation and (bottom) root mean square error between the observed and hind-casted TC frequencies in the WNP during peak season (July–October, JASO) for the initialization months from January to July (JFMAMJJ) using FLOR-FA. (top) The thick-dashed black line represents 0.05 level of significance.

landfalling/WNP TC frequency. In a Poisson model, the variance is equal to the mean. In this study, we assume that the Poisson random variable Y_i (i.e., the true number of TC frequency in the ith year) is independent from year to year and TC geneses are independent of one another in a specified year. This study trains the Poisson regression model with the observed total WNP TC frequency/TC landfall frequency and simulated large-scale circulation variables and then feed the trained model with the forecasted large-scale key parameters such as sea surface temperature (SST), 500 hPa geopotential height (Z500), vertical wind shear (VWS,$|U200-U850|$, U200 and 850 denote zonal wind at 200 and 850 hPa), and 850 hPa relative humidity (RH850), respectively.

2.5. TC Landfall Rate

TC landfall rate (ratio) is defined as the ratio of TC landfall frequency to the total WNP TC frequency [e.g., *Villarini et al*., 2012]. The complexity of TC landfall rate results from its dependence on both total TC and landfall frequency. This study focuses on the prediction of landfall frequency over East Asia, which can be obtained by summing up the landfall frequency over East Asia of the seven clusters.

$$\mathrm{Li} = \sum_{j=1}^{7} \mu_{ij}\tau_j, \tag{12}$$

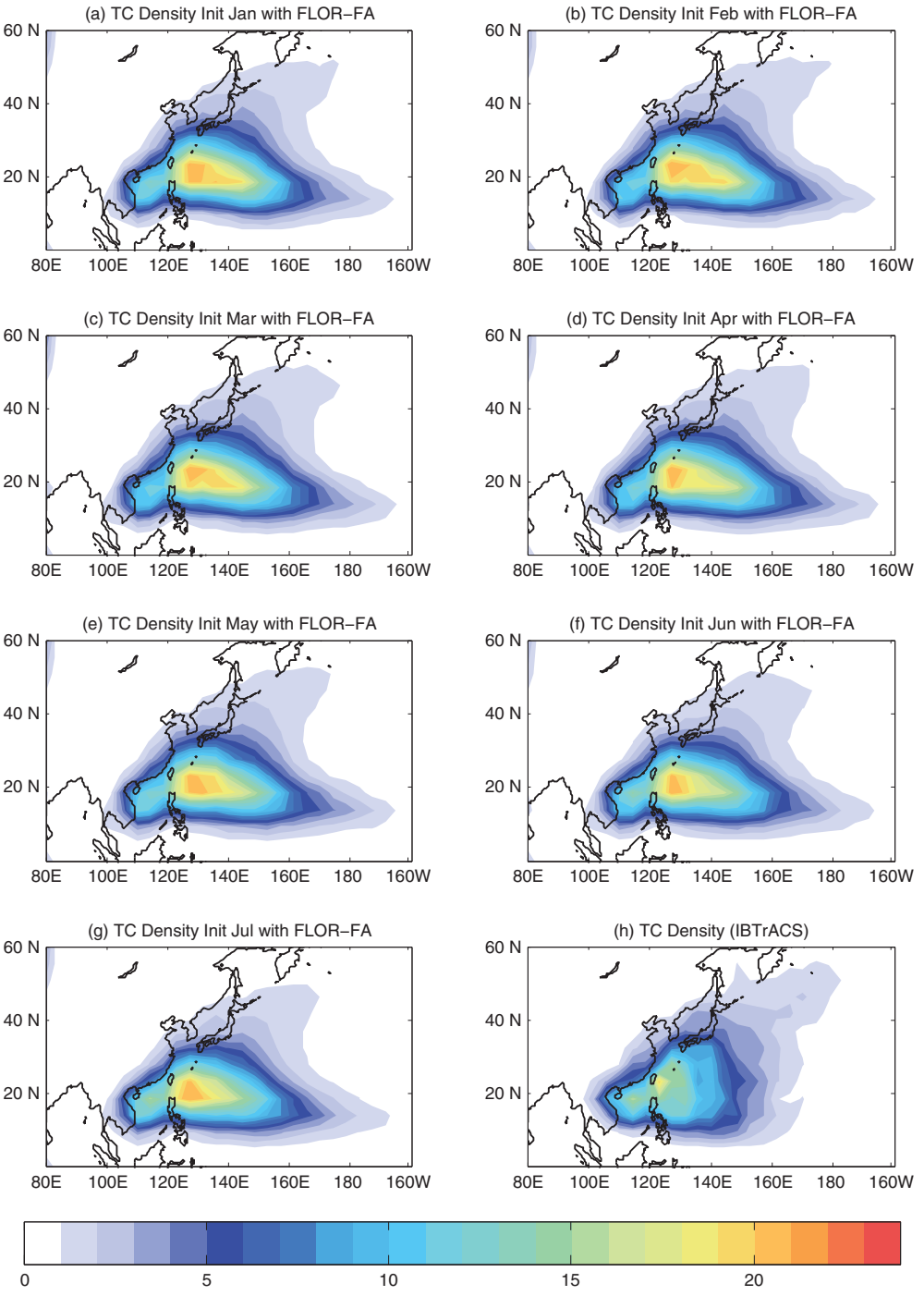

Figure 3. (a–g) The hind-casted TC track density (unit: times) with FLOR-FA initialized from January to July and (h) observed TC track density in the WNP for the period 1980–2013. The hind-casted TC track density is averaged over 12-ensemble members.

where L_i denotes the frequency of TC landfall over East Asia in the ith year, μ_{ij} the estimated TC frequency for cluster j in ith year using the hybrid models, and τ_j the landfall rate for cluster j.

2.6. TC Tracker

The tracker is developed to track TCs from 6 h climate simulations. This tracker has also been employed in *Zhang et al.* [2016a,2007] and *Murakami et al.* [2015]. The tracking processes are based on key atmospheric parameters such as air temperature, sea level pressure (SLP), and 10 m wind fields. The tracking procedures [*Murakami et al.*, 2015; *Zhang et al.*, 2016a,2016b] are described as follows.

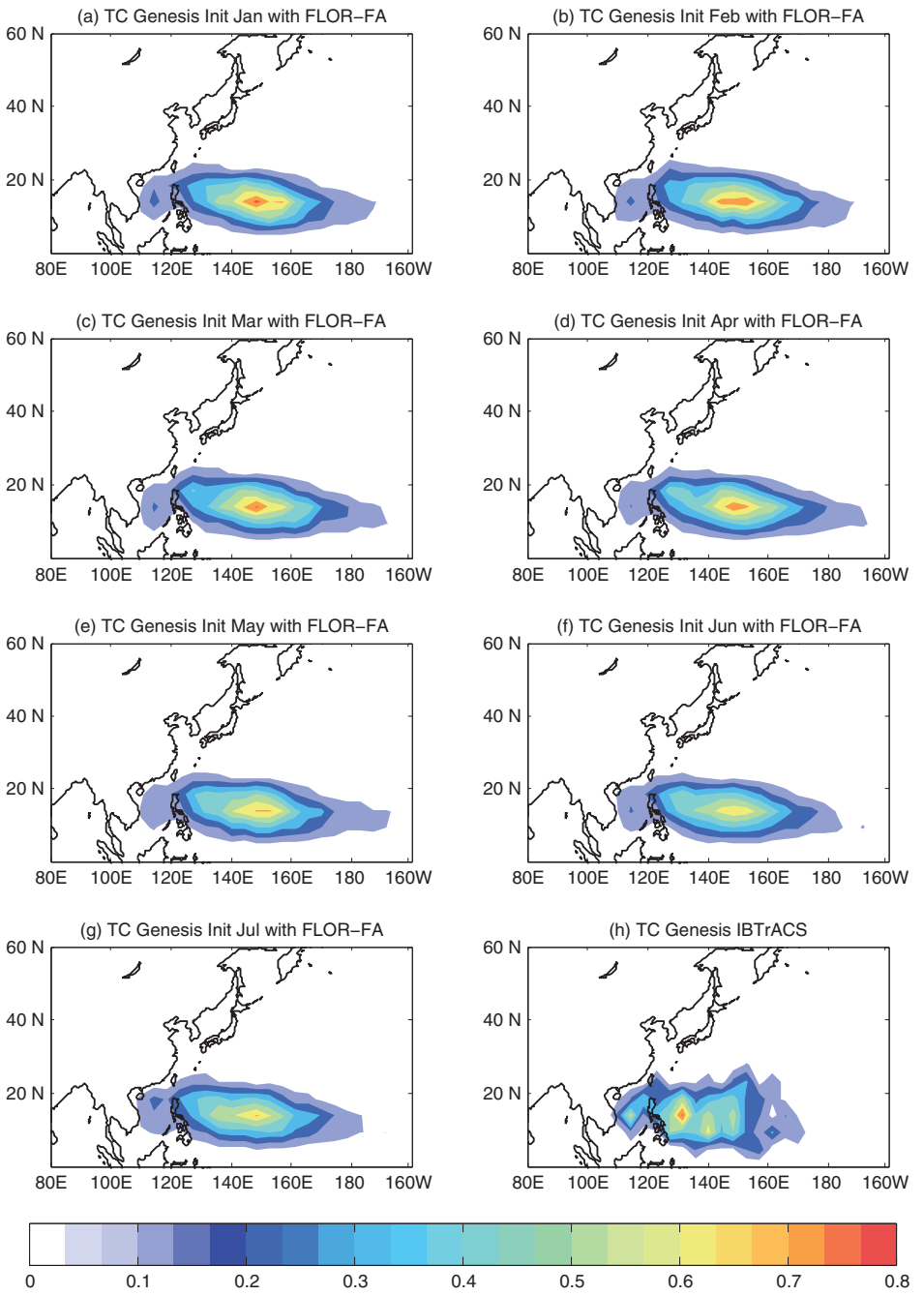

Figure 4. (a–g) The hind-casted TC genesis density (from July to October, unit: times) with FLOR-FA initialized from January to July and (h) observed TC genesis density in the WNP for the period 1980–2013.The hind-casted TC genesis density is averaged over 12 ensemble members.

1. Local minima are found from the SLP field. The spatial locations of the centers are adjusted by fitting a biquadratic function to the SLP.
2. Closed contours at an interval of 2 hPa (dp) are found around every single SLP low center. The Kth contour is marked as the contiguous region surrounding a low central pressure P with SLP lower than dp $\times$ K + P, detected by a "flood fill" algorithm. The contours are not necessarily circular. A maximum radius of 3000 km are searched from every single candidate low pressure center.
3. If closed contours are identified by the algorithm, the low is considered as a TC center. The tracker attempts to detect all closed contours surrounding the low center within certain distances from the low

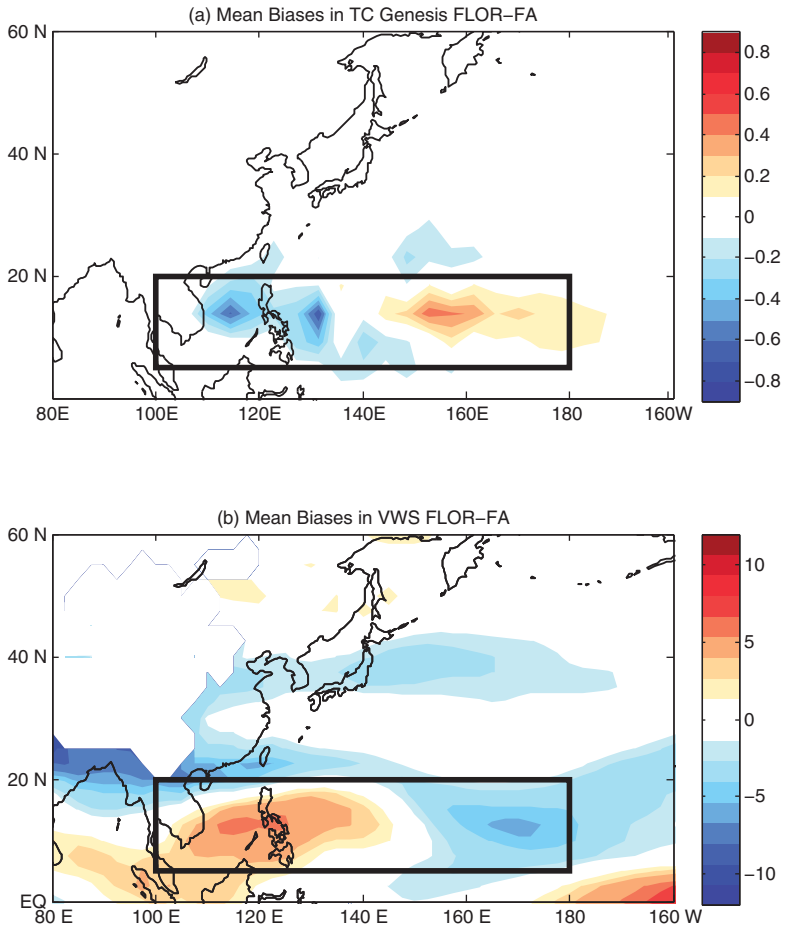

Figure 5. The (a) VWS (unit: ms^{-1}) and (b) TC genesis (unit: occurrences) biases in the WNP in FLOR-FA for the period 1980–2013 initialized from January to July.

center and without entering contours belonging to another low. The maximum 10 m wind within the set of closed contours is taken as the maximum wind speed (MWS) of the TC at that time.

4. Warm cores are identified by similar searching processes: closed 1°C contours are detected in the vicinity of the maximum temperature anomaly (t_a) within a TC's identified contours, less or equal to one degree from the low pressure center. This contour needs to have a radius smaller than 3°. If such a warm core cannot be found, it should not be considered as a warm-core low center.
5. TC centers are connected into a TC track by taking a low center at time T − dt, extrapolating the track forward dt, and then seeking TCs within 750 km. It is noted that a deeper low pressure center has higher priority of tracking.
6. The following criteria are further required to track the final TCs.
    1. At least 72 h of total detection lifespan (not necessarily consecutive).
    2. At least 48 cumulative (not necessarily consecutive) hours with a warm core.
    3. At least 36 consecutive hours of a warm core with winds stronger than 17.5 ms^{-1}.
    4. TC genesis should be located within equatorward of 40°N.

3. Forecasting Results

3.1. Results From FLOR-FA

Figure 2 depicts the predictive skill of WNP TC frequency from July to October (JASO) in FLOR-FA during the period 1980–2013. The predictions initialized in January, February, March, June, and July have statistically significant correlations with observations, while those in April and May are not significant at the 5% level (Figure 2a). Consistent with the correlation coefficients, the root mean square error (RMSE) between

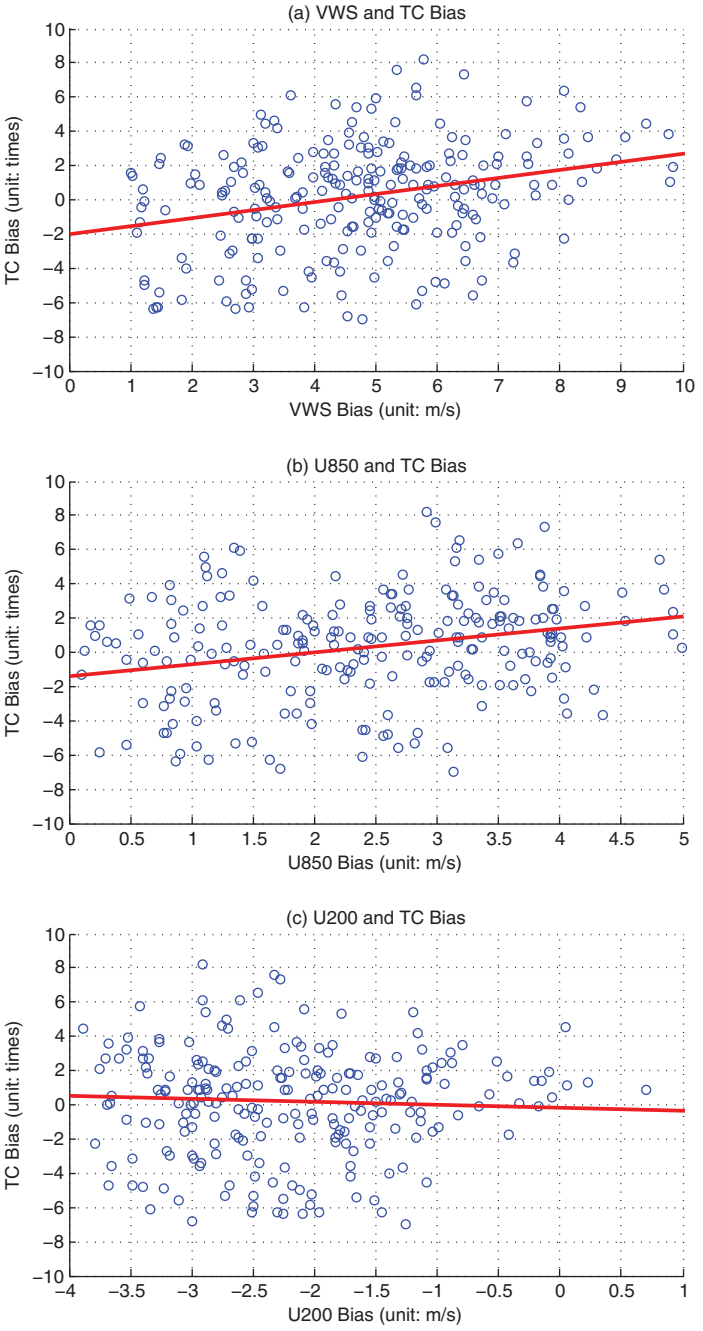

Figure 6. The scatter plots of the biases in (a) VWS (unit: m/s), (b) U850 (unit: m/s), U200 (unit: m/s), and those in WNP TC frequency of FLOR-FA predictions. The blue circles represent the annual values, with the red lines representing the linear fit.

predicted and observed TC frequency is high in April and May and low in the other initialization months (Figure 2b). By comparing the correlations and RMSE, the predictive skill initialized in January and February appears to be slightly better than that initialized in June and July (Figure 2). The larger the RSME, the more distinct the differences between observed and predicted WNP TC frequencies. The biases in the WNP TC frequency are defined as the differences between total observed TCs and FLOR-predicted TCs, with one value per year for the period 1980–2013 for the 12 ensemble members.

Figure 3 illustrates hind-casted (initialized from January to July) and observed TC track densities. TCs in FLOR-FA are tracked from the 6 hourly model output by using the tracker developed at GFDL as implemented in previous studies and the tracker is described in detail in subsection 2.5 [e.g., *Murakami et al.*, 2015; *Zhang et al.*, 2016a,2016b]. TC density is obtained by binning the 6 hourly TC tracks in the WNP into 5 × 5° grid boxes without smoothing. The hind-casted TC track density captures fundamental structures of observations for all initialization months (Figure 3), though there are positive biases in TC density in the region 120°E–140°E for the prediction with FLOR-FA (Figure 3). The predicted TC density for different initialization months shows similarity with one another (Figure 3). The hind-casted TC genesis density initialized from January to July resembles observations in magnitude while the spatial patterns are different because the high center of TC genesis density in FLOR-FA is shifted eastward in contrast to observations (Figure 4). There is a high center of TC genesis in 135°E in the observations while the high center of TC genesis in the FLOR-FA hindcasts is located at145°E (Figure 4), suggesting an eastward shift in the climatology of TC genesis with FLOR-FA.

For further assessment, we find that the spatial pattern of biases of predicted VWS in the WNP are significantly associated with that in the WNP TC frequency (Figure 5), suggesting that the VWS biases may play an important role in explaining the WNP TC frequency biases. The scatter plot between VWS biases and TC

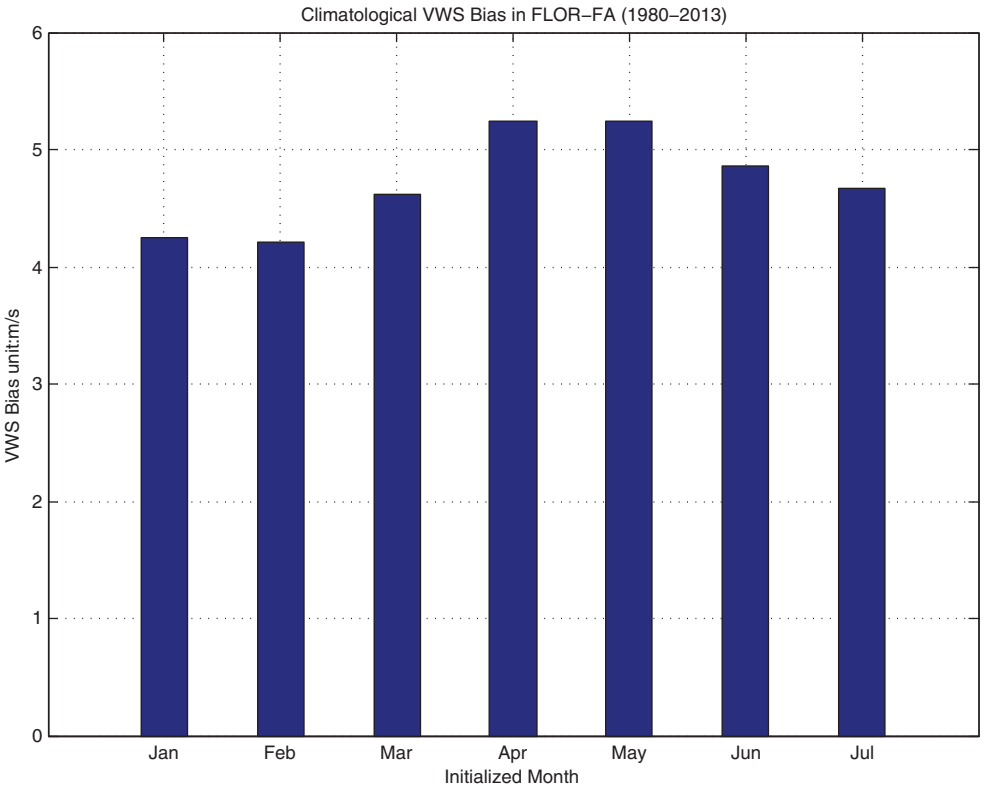

Figure 7. The VWS (unit: m/s) biases in the WNP in FLOR-FA for the period 1980–2013 initialized from January to July.

frequency biases for 1980–2013 further supports this linkage (Figure 6a). However, the biases of other predicted variables (i.e., SST, Z500, and RH850) are not associated with those of WNP TC frequency (figure not shown). Further analysis shows that the biases in predicted VWS come mainly from U850 but not from U200 (Figures 6b and 6c). It is noted that the biases in predicted large-scale parameters (e.g., VWS) are calculated by the differences in the climatology in FLOR-FA and observations. Therefore, large biases in a predicted parameter may not necessarily be related to low correlation coefficient between the observation and prediction of this parameter. Moreover, the changes in VWS biases (Figure 7) are consistent with the changes in correlation and RMSE of WNP TC frequency for different initialization months (Figure 2). In other words, the VWS biases are large when predictions are initialized in April and May while they are small in the other initialization months (Figure 7), further suggesting that the VWS biases may play an important role in explaining the predictive skill of FLOR-FA for WNP TC frequency in different initialization months (Figure 2).

If we use large-scale parameters simulated by dynamic models to predict WNP TC frequency, the dynamic model should have significant forecast skill in predicting these potential large-scale parameters, at least over the selected spatial domains. Figure 8 illustrates the predictive skill of potential predictors (e.g., SST, Z500, VWS, U850, and RH850) initialized in January which is represented by the correlation between observed and predicted values at each grid (Figure 8). Those potential variables have been widely used to predict WNP TC frequency and are closely relevant to TC genesis [e.g., *Chan et al.*, 2001; *Kwon et al.*, 2007; *Li et al.*, 2013]. The spatial correlation maps initialized from February to July are provided in supporting information Figures S1–S6. The spatial correlation map for SST covers the global ocean while those for atmospheric large-scale parameters (e.g., VWS and Z500) are confined in the Pacific because remote SST anomalies can also modulate WNP TC frequency [*Zhan et al.*, 2010; *Li et al.*, 2013; *Yu et al.*, 2015]. The predictive skill of SST is high in most of the Pacific, the Atlantic, and the Indian Oceans with FLOR-FA (Figure 8). Though the correlation maps between the predicted and observed potential predictors are similar when initialized from January to July (supporting information Figures S1–S6), the predictive skill for the potential predictors using FLOR-FA is slightly higher when closer to target month (JASO, Figure 8 and supporting information Figures S1–S6). The covariate Z500 is highly predictable, especially in the tropics (Figure 8); VWS is highly predictable in the Pacific region (Figure 8), while

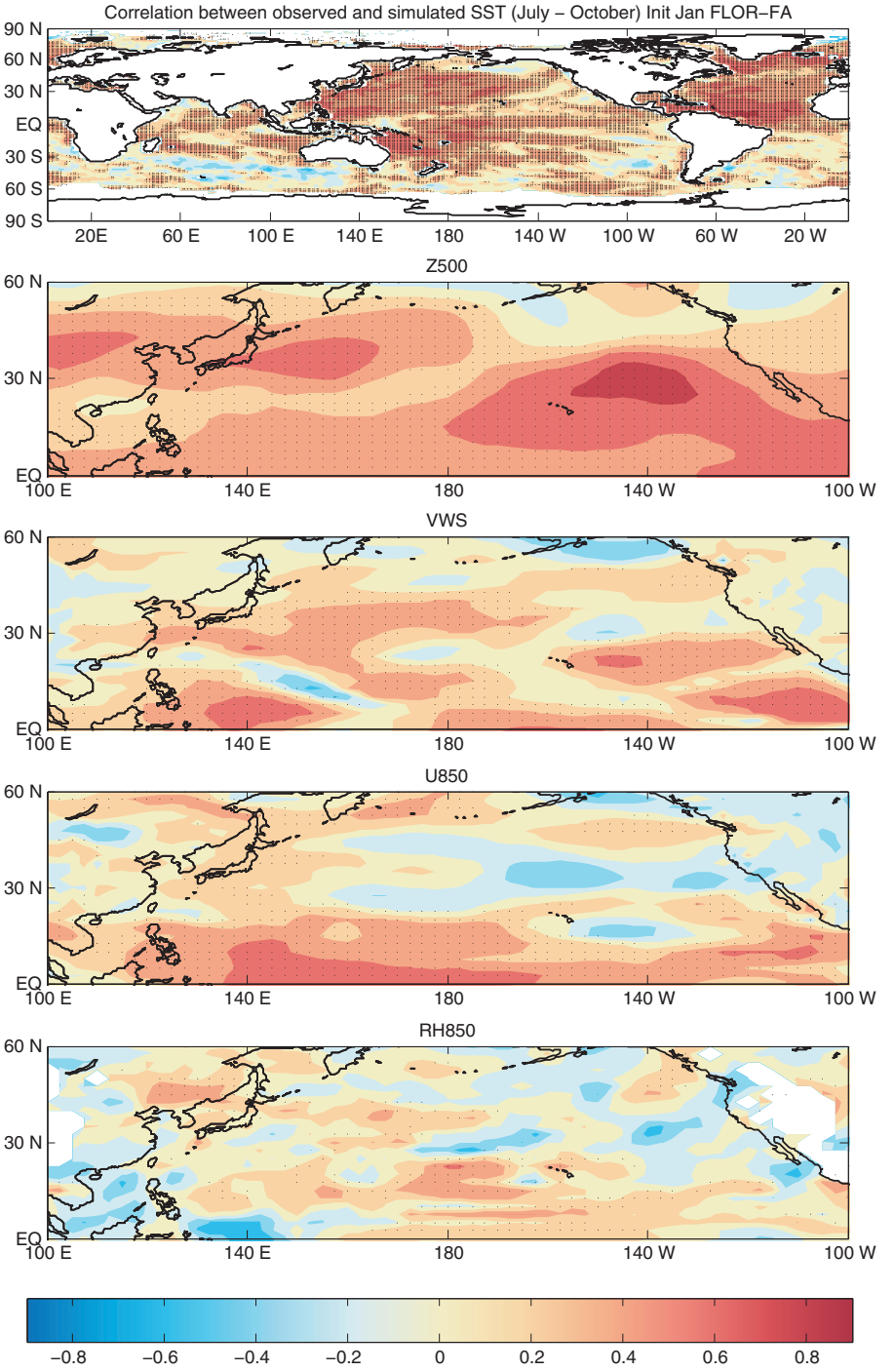

Figure 8. The correlation between hind-casted (initialized in January) and observed potential predictors (SST, Z500, VWS, U850, and RH850) during the peak season (JASO) to represent the predictive skill of the variables using FLOR-FA. Stippled black regions are those with 0.05 level of significance.

U850 is marginally predictable in a small region of the Pacific and generally located in the tropics. The 850 hPa relative humidity is, however, predictable only in limited regions in the WNP in FLOR-FA (Figure 8). FLOR-FA cannot simulate well 850 hPa relative humidity, which is an important factor for TC genesis. The poor performance of FLOR-FA in simulating RH850 may limit its capability in forecasting WNP TC frequency. We therefore select SST, Z500 and VWS as potential predictors for the hybrid model due to the high predictive skill with dynamic-model predictions (FLOR-FA).

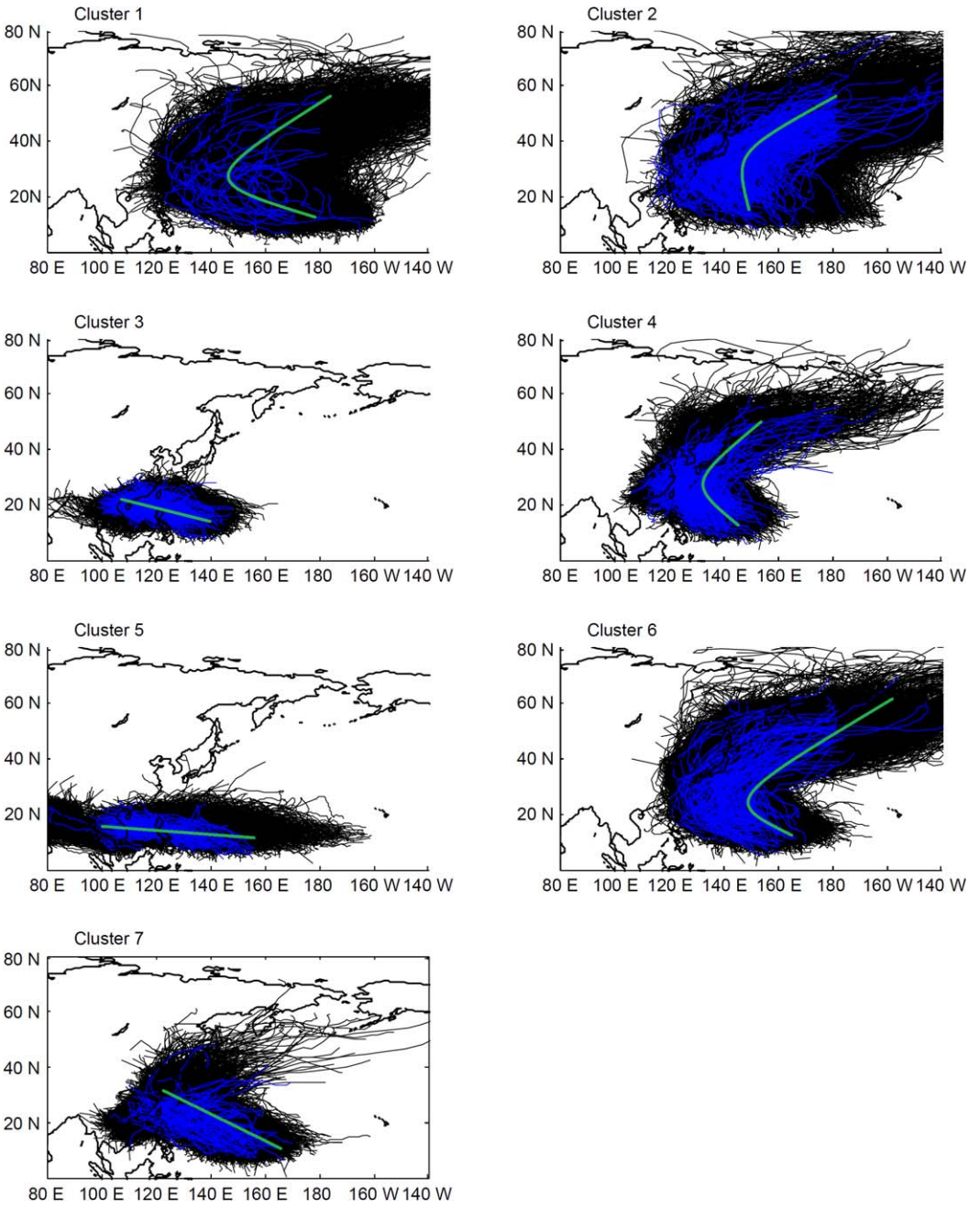

Figure 9. The seven clusters of observed TC tracks and 12-ensemble hind-casted TC tracks with FLOR-FA of the seven predictions initialized from January to July unraveled by finite-mixture-model-based cluster analysis. The black curves represent the hind-casted TC tracks while the blue curves the observed TC tracks in the period 1980–2013. The thick green line or curves represent mean curves of the clusters.

3.2. Results From the Hybrid Model

The FMM-based cluster analysis unravels hidden and important patterns from TC tracks, which are potentially useful to predict basin-total TC frequency and landfall over East Asia. This subsection focuses on the cluster analysis of historical and predicted TC tracks, predicting the identified seven clusters, and subsequently making skillful prediction for total WNP TC frequency and landfalls over East Asia.

3.2.1. Cluster Analysis

The FMM-based cluster analysis is used to identify seven clusters from the combined historical and predicted TC tracks (Figure 9). The reason for this cluster analysis is twofold: (1) it enables the evaluation of

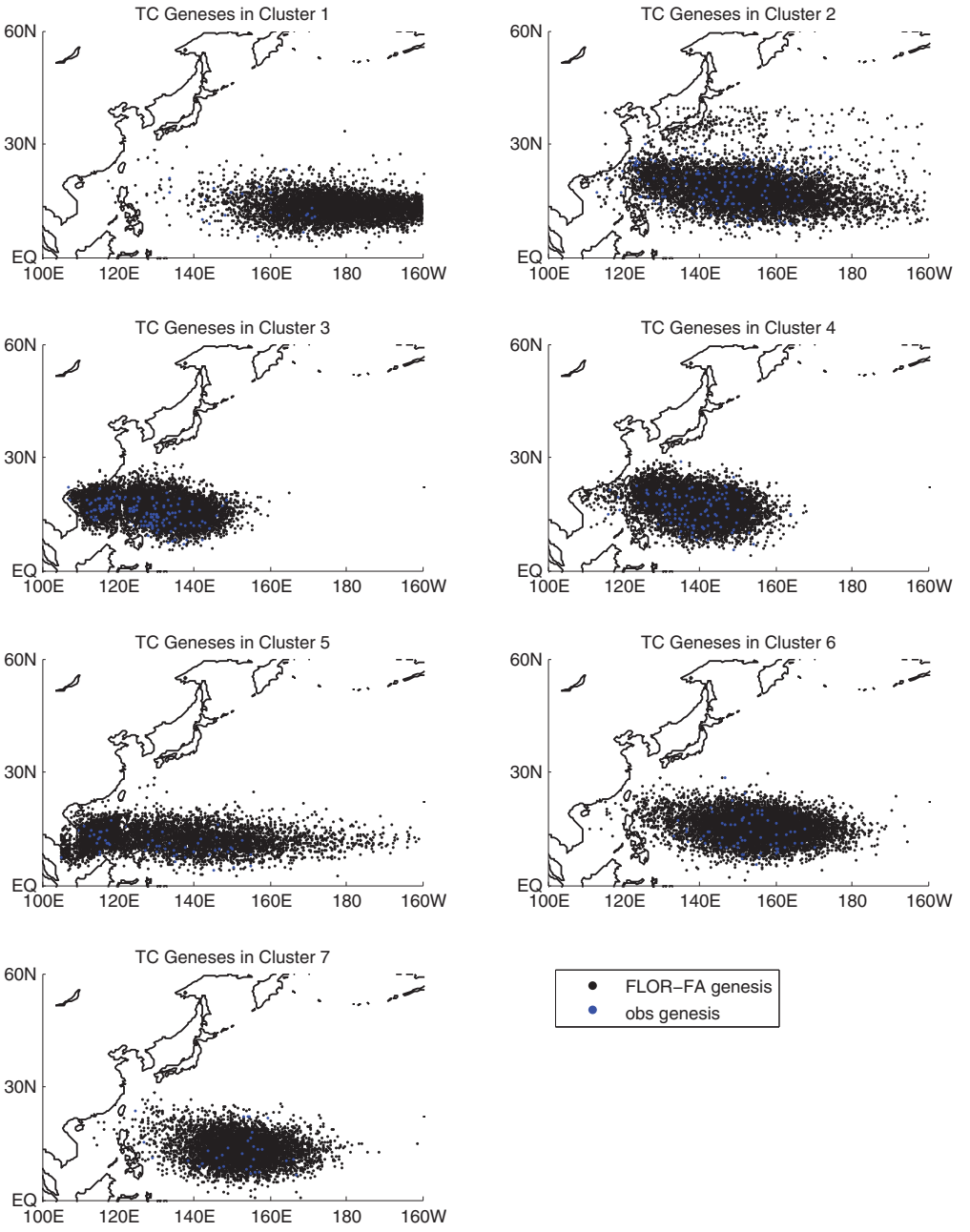

Figure 10. TC geneses in 12-member forecasts with FLOR-FA initialized in January to July (black dots) and in the observations (blue dots).

predictability for each cluster with FLOR-FA; (2) it allows assessing whether the clusters in historical and predicted TC tracks are consistent. Because we have 12 ensemble members and 7 initialization months (i.e., January–July) for the predictions with FLOR-FA (12 × 7 × 34 years), the predicted TC tracks are much more than the observed ones (1980–2013, 34 years) (Figure 9). Our cluster analysis results are overall consistent with *Camargo et al*. [2007a]; there are four straight-moving and three recurving clusters in *Camargo et al*. [2007a] while there are three straight-moving and four recurving clusters in the present study (Figure 9). The main difference is that we have one more recurving cluster (cluster 2 in Figure 9) than *Camargo et al*. [2007a], which may arise from more TCs moving to extratropics in FLOR-FA. We speculate that more recurving TCs that move in the extra-tropics in FLOR-FA are associated with the eastward-shift TC genesis locations in FLOR-FA which has been documented in *Vecchi et al*. [2014]. Due to the eastward-shift TC genesis, TCs have more chance to stay on the open seas. Most of TCs first move northwestward toward the

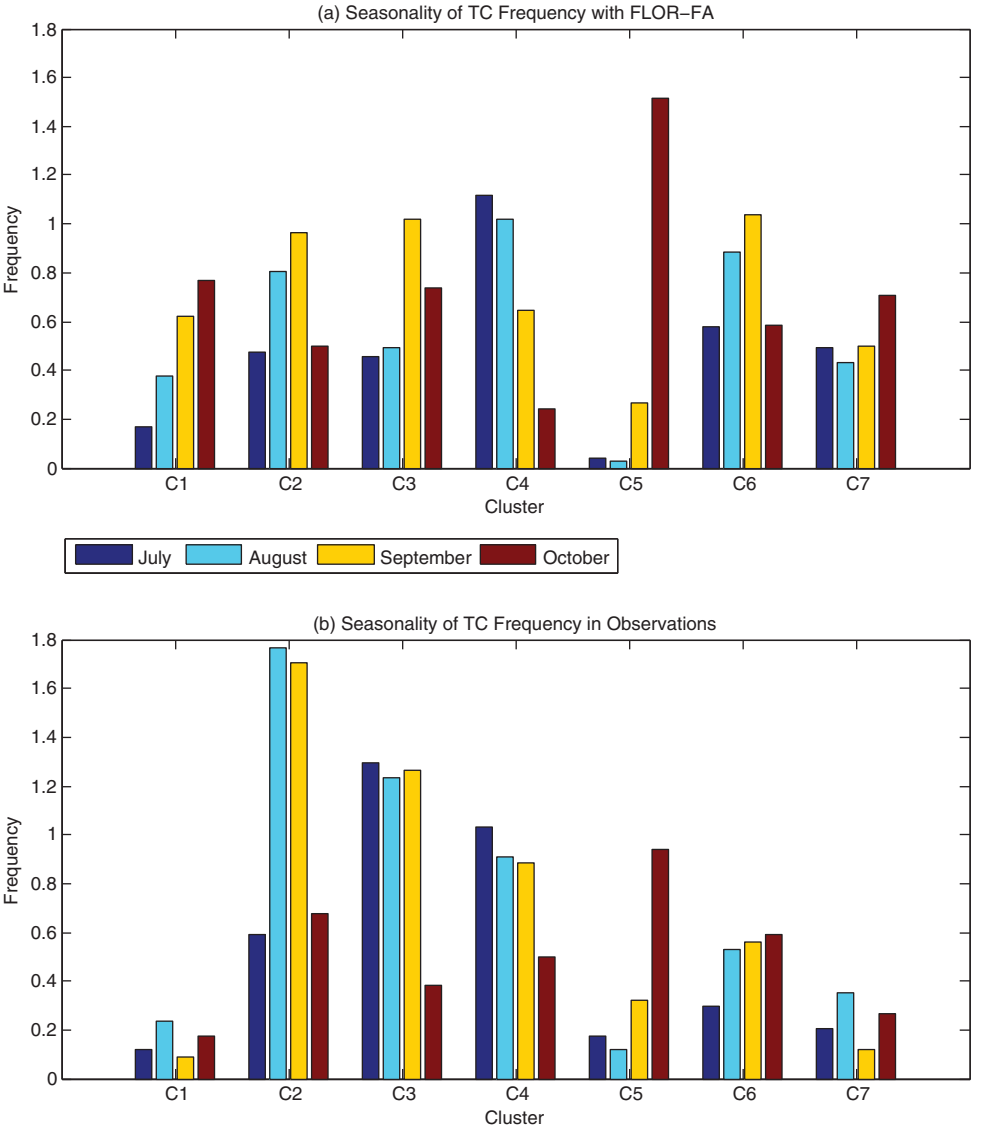

Figure 11. Seasonality of WNP TCs in (a) FLOR-FA and (b) the observations in the peak TC season (July–October, JASO).

extratropics after they are formed due to Beta effect [*Holland et al.*, 1983]. Given the eastward-shift geneses, TCs tend to move into extratropics and recurve due to strong westerly in the midlatitudes.

Further analysis of the seven clusters includes their genesis locations, frequency (percentage), maximum intensity, landfall frequency, and seasonality of TCs in each cluster in the ensemble forecasts of FLOR-FA and observations following *Daloz et al.* [2015]. Figure 10 illustrates the TC geneses of seven clusters with FLOR-FA in 12 members and 7 initial months and those in the observations. TC geneses in the observations capture the characteristics of FLOR-FA well in the seven clusters (Figure 10). However, there is a marked eastward shift in the TC geneses of FLOR-FA for almost all seven clusters (Figure 10), consistent with previous studies [e.g., *Vecchi et al.* 2014].

Table 1 shows the frequency (percentage), genesis locations, landfall frequency, and maximum intensity in the seven clusters of FLOR-FA and observations, respectively. The climatological TC frequencies during peak season (JASO) in clusters 4, 5, and 6 are similar between FLOR-FA and observations. There are higher TC frequency in clusters 1 and 7 and lower TC frequency in cluster 2 in the hindcasts of FLOR-FA than the observations. The climatology of TC genesis locations in FLOR-FA is basically consistent with that in the observations, except for an eastward shift (Table 1), as also shown in Figure 10. The

Table 1. The Number (Percentage) of TCs, Genesis Locations, Landfall Frequency Over East Asia and Average Maximum Intensity in Each Cluster in FLOR-FA and the Observations

CTL	Data Set	C1	C2	C3	C4	C5	C6	C7
No. of TC per year	FLOR-FA	1.9 (11.7%)	2.7 (16.6%)	2.7 (16.5%)	3.0 (18.4%)	1.8 (11.0%)	2.1 (12.9%)	2.1 (12.9%)
	OBS	0.6 (3.5%)	4.7 (27.2%)	4.2 (24.3%)	3.3 (19.1%)	1.6 (9.2%)	2.0 (11.6%)	0.9 (5.1%)
Genesis locations (Lon, Lat)	FLOR-FA	(176.4,13.2)	(151.3,18.2)	(128.9,16.6)	(139.5,17.0)	(134.1,12.4)	(154.8,15.3)	(152.3,13.5)
	OBS	(156.0,13.7)	(145.6,19.2)	(126.7,15.2)	(138.3,16.1)	(130.4,10.8)	(152.0,14.0)	(150.6,12.9)
Landfall (East Asia)	FLOR-FA	0.3	0.9	2.4	2.3	1.7	1.2	1.3
	OBS	0.3	1.6	3.9	2.5	1.5	0.7	0.8
Maximum intensity	FLOR-FA	29.7	28.9	27.1	28.3	30.0	29.6	30.8
	OBS	38.3	31.0	27.2	34.6	34.2	35.1	43.3

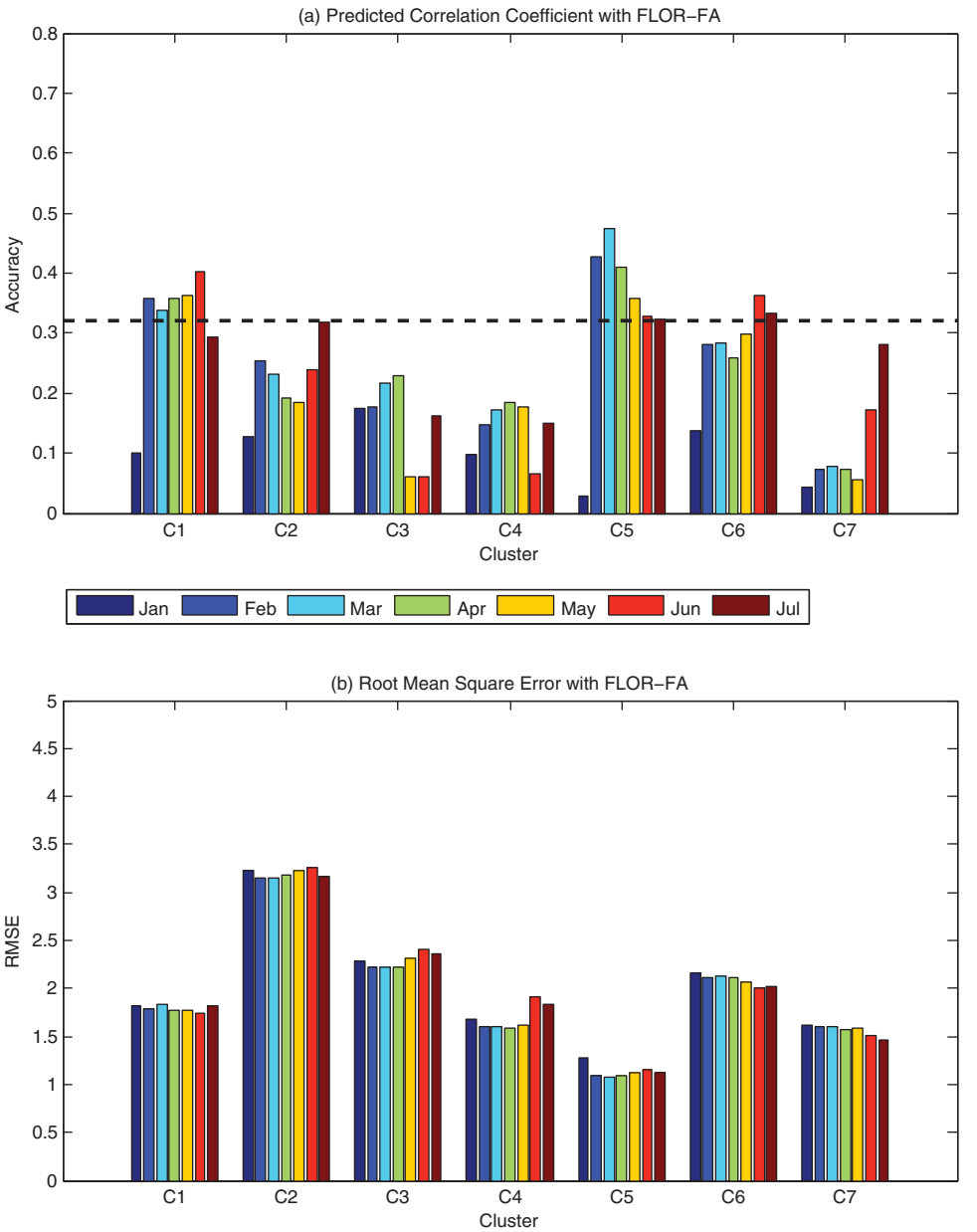

Figure 12. Correlation and root mean square error of WNP TC frequency in observed and hind-casted seven clusters (i.e., C1, . . ., C7) produced by FLOR-FA initialized from January to July (bars with different colors). (top) The thick-dashed black line represents the 0.05 level of significance.

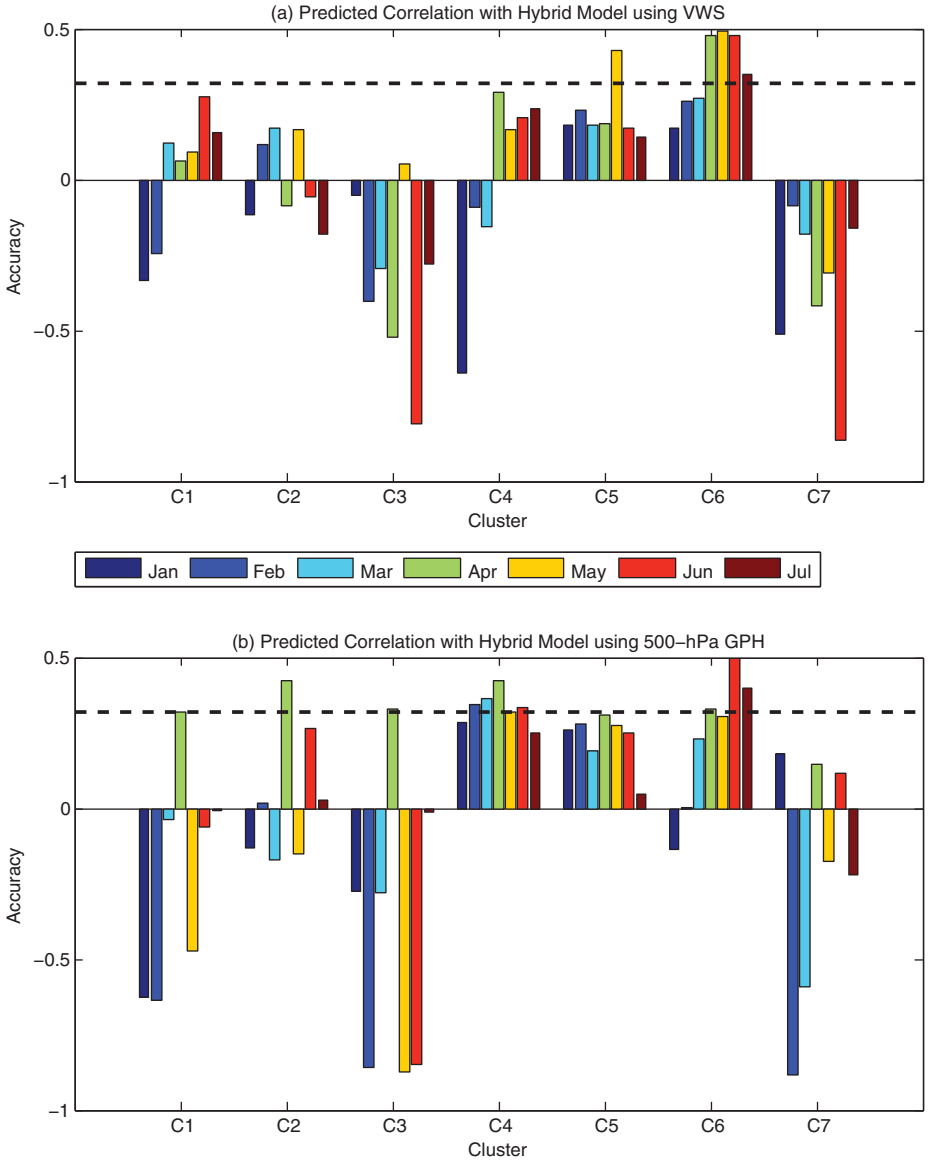

Figure 13. The prediction skill of the hybrid models based only on (a) VWS and (b) Z500 for different initialization months and clusters. The domains for VWS or Z500 are selected such that the correlations between observed TC frequency and simulated values of VWS/Z500 are significant at the 5% level. The thick-dashed black lines in represent the 0.05 level of significance.

frequencies of TC landfalls over East Asia in FLOR-FA are similar to those in the observations except for cluster 3 in which FLOR-FA has 1.5 landfalls more than the observations (Table 1). The climatology of maximum intensity in FLOR-FA is lower than in the observations for all seven clusters (Table 1). Previous studies have reported that weaker TCs in FLOR-FA are in part due to the lower spatial resolution, which has been much improved in a high-resolution FLOR (HiFLOR) with 25 km spatial resolution of its atmospheric component [e.g., *Vecchi et al.*, 2014; *Murakami et al.*, 2015; *Zhang et al.*, 2016b]. The seasonality of TCs in FLOR-FA are generally consistent with that in the observations (Figure 11). Clusters 1 and 7 of FLOR-FA have more TCs than those in the observations during September and October, while clutsers 2 and 3 of FLOR-FA have less TCs than those in the observations during August and September (Figure 11). Therefore, the seven clusters in FLOR-FA are overall consistent with those in the observations in terms of genesis locations, TC frequency (percentage), landfall frequency, maximum intensity, and seasonality, though there is still inconsistency in some clusters. This lends credence to the application of cluster analysis results using TCs from both the hindcasts of FLOR-FA and the observations to build a hybrid model for seasonal forecasting.

Table 2. The Domains (rectangle: lon1, lon2, lat1, lat2) Selected for SST, Z500, and VWS for Different Clusters

Cluster	SST	Z500	VWS
C1	[120°E 145°E 10°N 20°N] [163°W 133°W 20°S 10°S] [160°E 150°W 20°N 40°N]	None	None
C2	[130°E 80°W 10°S 10°N] [60°W 20°W 10°N 30°N]	None	None
C3	[50°W 15°W 50°N 63°N]	None	None
C4	[130°E 155°W 30°N 50°N] [160°E 130°W 40°S 8°S] [60°W 10°W 15°N 60°N] [38°E 108°E 50°S 10°S]	[100°E 180 30°N 50°N]	None
C5	[125°E 160°W 20°N 40°N] [160°E 130°W 40°S 8°S] [90°W 20°W 10°N 25°N] [38°E 108°E 50°S 10°S]	[140°E 140°W 10°N 45°N]	None
C6	[135°E 145°W 25°N 55°N] [155°E 90°W 15°S 15°N] [155°E 135°W 35°S 15°S] [160°W 90°W 65°S 40°S] [70°W 10°W 0 68°N] [38°E 110°E 50°S 10°S]	[100°E 110°W 5°N 60°N]	[110°E140°W 5°N 40°N] [165°E145°W 5°N 20°N] [125°E160°E 5°N 15°N]
C7	[160°E 90°W 15°S 15°N] [180°E 90°W 65°S 40°S] [180°E 90°W 35°S 20°S]	None	None

The seven clusters capture fundamental characteristics of TC tracks in the WNP (Figure 9). The correlations between observed and predicted WNP TC frequency are positive for each cluster in all initialization months (Figure 12). For clusters 1 and 5, FLOR-FA shows relatively high skill for predicting WNP TC frequency; most of the correlations between observed and predicted TC frequency in those clusters are significant at the 0.05 level (Figure 12). However, the correlations for clusters 2, 3, 4, 6, and 7 fail to pass the significance test at 0.05 level. Furthermore, the RSME between observed and predicted TC frequency for clusters 1, 4, 5, and 7 are low (Figure 12). Cluster 2 has the highest RSME, though the correlation is relatively high among the seven clusters. The high RMSE in cluster 2 (i.e., the northward-moving cluster) is because there are three years (1984, 1988, 1989) in the observations with extremely high frequencies (10, 12, and 10 TCs). However, the TCs of cluster 2 in FLOR-FA are much less than those in the observations in those 3 years, leading to high RMSE values. This indicates that cluster 2 is relatively difficult to be predicted by FLOR-FA.

3.2.2. Prediction of Seven Clusters and Total WNP TC Frequency

To predict the frequency of TCs in each cluster, our strategy is to: (1) further select predictors for each cluster, (2) select spatial domains for the predictors for each cluster, (3) build statistical relationship between selected simulated large-scale variables (predictors: SST, Z500, and VWS) and observed TC frequency in each cluster using Poisson regression models, and (4) infer the predicted TC frequency from the built statistical relationship using simulated large-scale variables.

The spatial correlation maps (Figure 8 and supporting information Figures S1–S6) are considered as an important factor to select the predictors for the hybrid model. SST is always selected because previous studies have demonstrated its importance in modulating the genesis, development, and track of WNP TCs. To further select predictors in addition to SST for each cluster, we build hybrid models using a single predictor (VWS/Z500) in the domains where the correlations between observed TC frequency and simulated large-scale parameters are significant. Results show that VWS exhibits some skill for cluster 6 while Z500 works well only for clusters 4, 5, and 6 (Figure 13). *DelSole and Shukla* [2009] reported that one may obtain artificial skill if the regions without physical meanings are used to build seasonal forecasting models. Therefore, we only select the regions with physical meanings from the literature for the predictors. We determine the spatial domains for the predictors based on both geographical locations and physical meanings for each cluster (Table 2). The candidate domains are first selected based on the spatial correlation between observed TC frequency and large-scale parameters. In general, the spatial domains for VWS and Z500 should be located in the Pacific, while those for SST do not necessarily have to be located in the Pacific because various studies have indicated that SST gradients and remote SST anomalies can influence TC frequency in the WNP

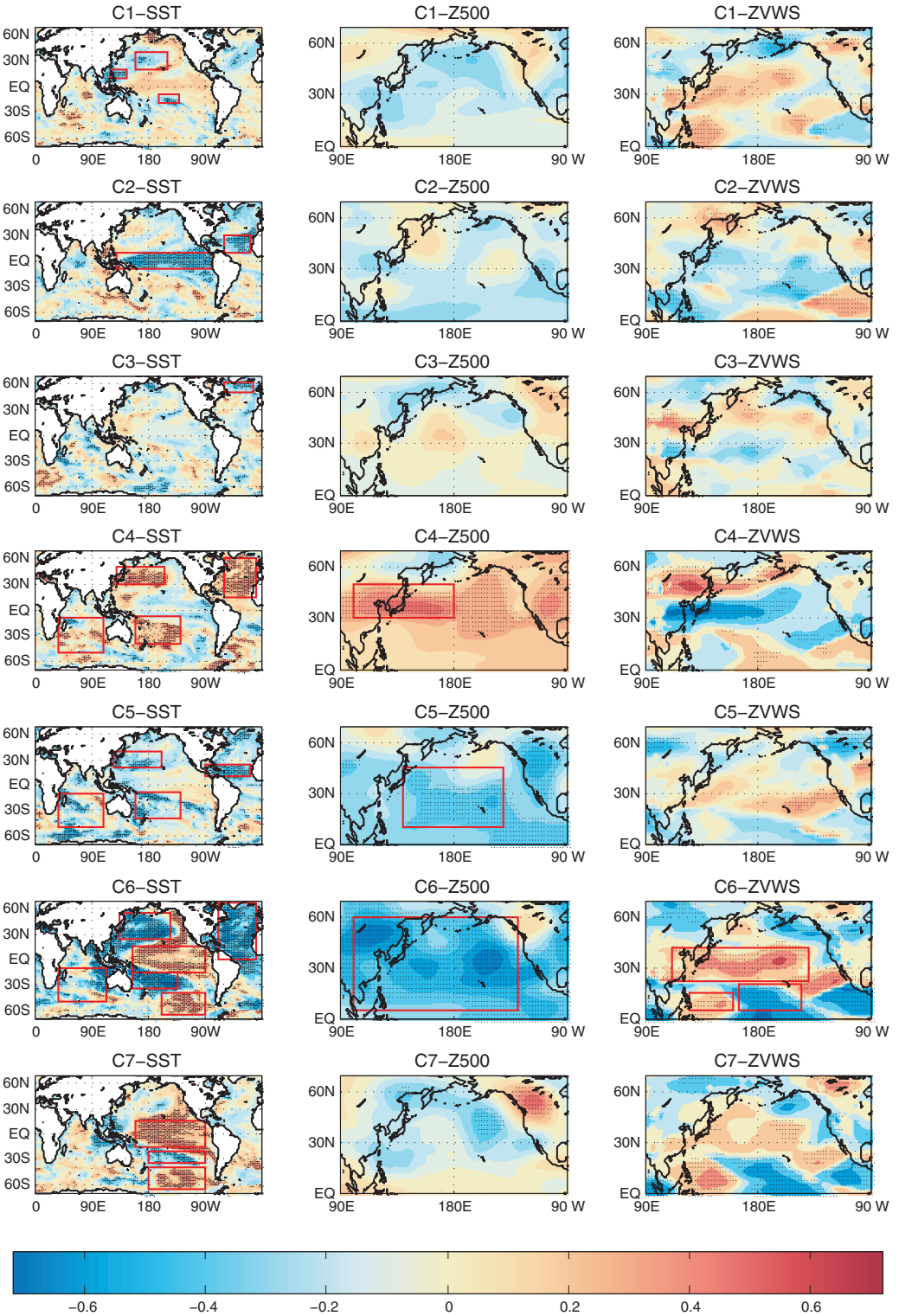

Figure 14. The spatial correlation domains (red rectangles) of the three predictors (SST, Z500, and VWS) for the seven clusters (C1,. . .,C7) initialized from January to July. Stippled regions are those with 0.05 level of significance. The shading represents correlation coefficients between observed TC and simulated variables.

[e.g., *Zhan et al*., 2010; *Yu et al*., 2015]. Previous studies have also indicated that SST in the Pacific [*Wang and Chan*, 2002; *Camargo and Sobel*, 2005], the Indian [*Du et al*., 2010; *Zhan et al*., 2010], and the Atlantic [*Huo et al*., 2015; *Yu et al*., 2015] Oceans can modulate WNP TC activity.

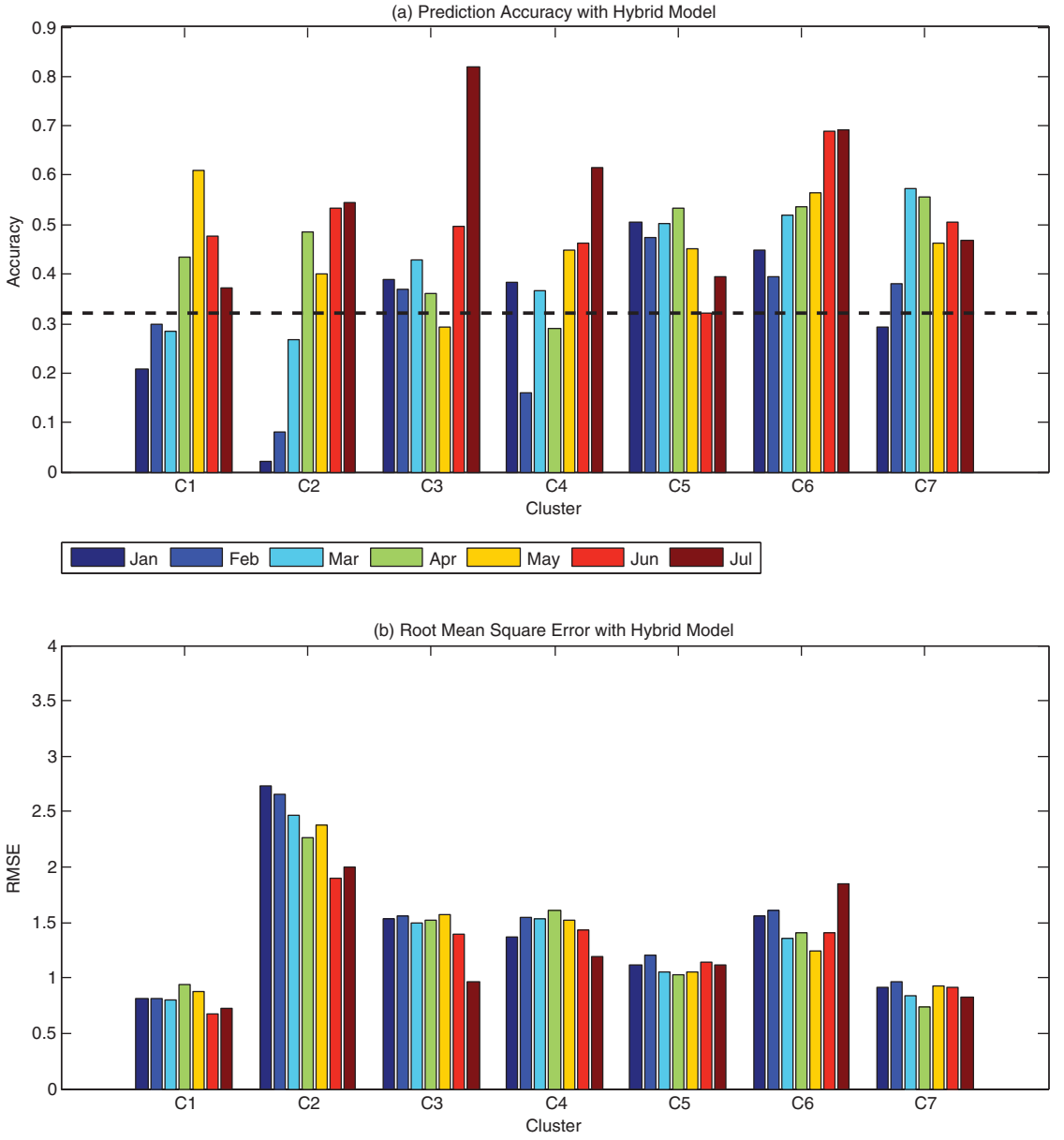

Figure 15. Correlation and RMSE values of observed TC frequency and hybrid-model initialized from January to July for each cluster by leave-one-out cross validation. (top) The thick-dashed black line represents the 0.05 level of significance.

The candidate areas are added one by one, and only the rectangles that can add values to the prediction skills are retained. For a predictor (e.g., SST), there may have several spatial domains with respect to a cluster. In other words, after we select a rectangle for the predictor, a hybrid model is built based on average predictor values in that rectangle (we add predictor values when the correlation coefficient in a grid is positive, and subtract the predictor value when the correlation coefficient in this grid is negative) as a predictor. If the prediction skill of this hybrid model is significant, we retain this rectangle, otherwise we discard it. By doing this, the selected rectangles are important to predict TC frequency in different clusters. The predictors and domains for each cluster are shown in Figure 14 and listed in Table 2.

The spatial domains for each variable are justified in terms of physical mechanisms by previous studies. We select three regions for SST related to cluster 1 (Figure 14). The two regions in the North Pacific are associated with the western part of the El Niño Southern Oscillation (ENSO) or the Pacific Decadal Oscillation (PDO) [*Wang and Chan*, 2002; *Camargo and Sobel*, 2005; *Zhang et al*., 2013e] while the region in the

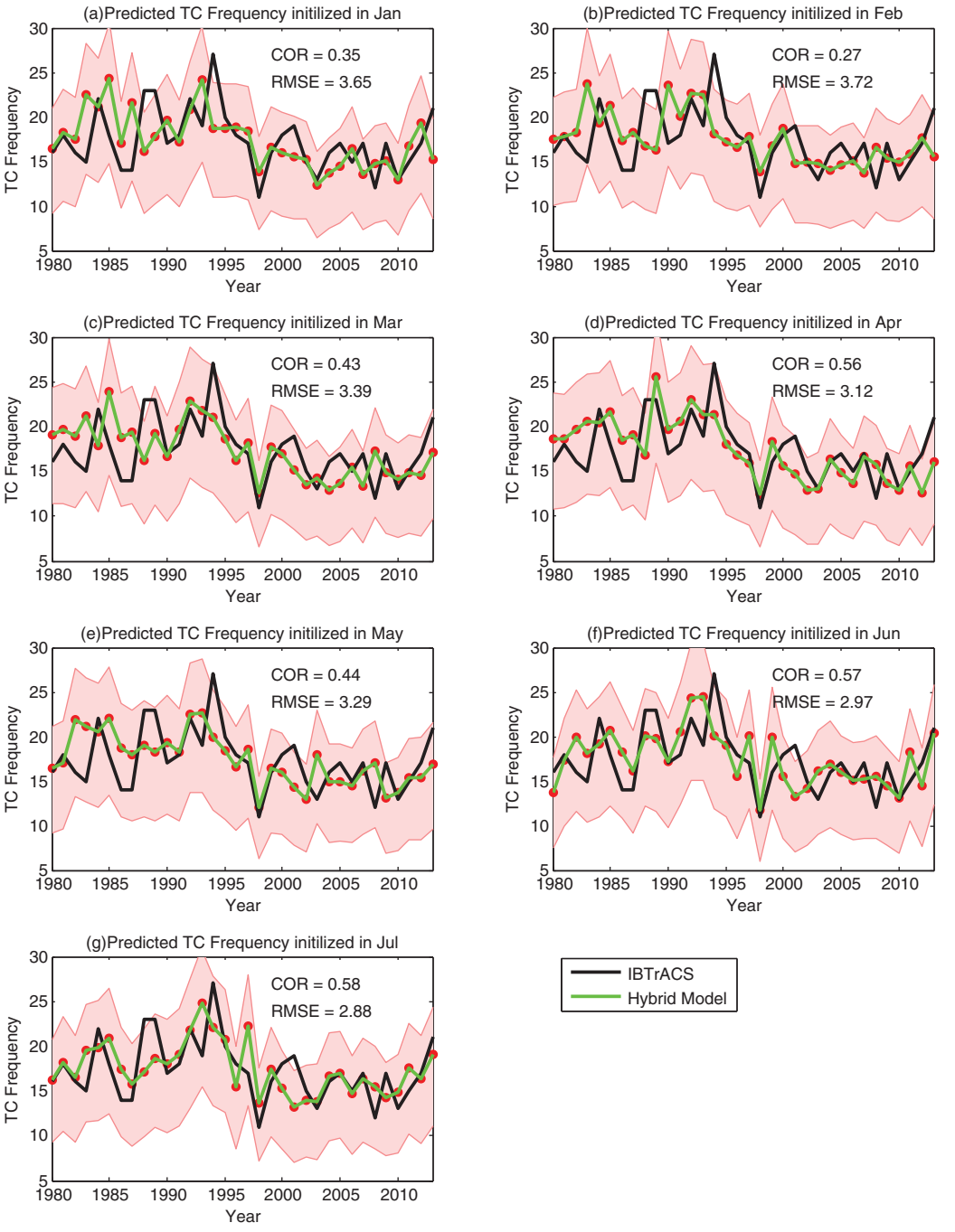

Figure 16. Correlation and RMSE of observed and hind-casted WNP TC frequency produced by the hybrid model after leave-one-out cross validation. The red circles denote the predictions of WNP TC frequency in each year using the hybrid model, while the black solid lines represent the observations. The pink areas represent the 10% and 90% percentiles of 1000 random sampling of TC frequency given μ (the predicted mean TC frequency) under Poisson distribution.

Southwestern Pacific is relevant to the SST gradient between the southwestern Pacific and the western Pacific warm pool reported in *Zhan et al.* [2013] (Figure 14). Two regions for SST related to cluster 2 are located in the tropical Pacific (La Niña-like pattern) [*Wang and Chan*, 2002; *Camargo and Sobel*, 2005] and North Atlantic [*Li et al.*, 2013; *Huo et al.*, 2015; *Yu et al.*, 2015]. The SST region related to cluster 3 is located in the North Atlantic with the spatial pattern similar to the Atlantic tripole mode [*Deser and Timlin*, 1997], although the correlations in the tropical Atlantic are not statistically significant. The association between the Atlantic tripole mode and WNP TC activity could be supported by previous studies [*Li et al.*, 2013; *Huo*

Table 3. The Equations for the Hybrid Model of Clusters Initialized in January[a]

Equations	Initialized in January
Cluster 1	$\mu_{i1} = \exp(-0.5725 + 3.4985 \cdot SST_i)$
Cluster 2	$\mu_{i2} = \exp(1.5464 + 0.4045 \cdot SST_i)$
Cluster 3	$\mu_{i3} = \exp(1.4159 + 0.9178 \cdot SST_i)$
Cluster 4	$\mu_{i4} = \exp(1.1724 + 1.4646 \cdot SST_i - 0.0044 \cdot Z500_i)$
Cluster 5	$\mu_{i5} = \exp(0.3453 + 6.8851 \cdot SST_i - 0.0244 \cdot Z500_i)$
Cluster 6	$\mu_{i6} = \exp(0.5332 + 1.8980 \cdot SST_i - 0.0029 \cdot Z500_i - 1.0555 \cdot VWS_i)$
Cluster 7	$\mu_{i7} = \exp(-0.1035 + 2.1759 \cdot SST_i)$

[a]The parameter μ_{i1} represents the estimated TC frequency in cluster 1 in the *i*th year, and the others are defined likewise.

et al., 2015; *Yu et al*., 2015]. The Atlantic Meridional Mode strongly modulates WNP TC activity in both observations and a suite of FLOR-FA experiments; negative (positive) AMM phases are conducive to more (less) WNP TCs [*Zhang et al*., 2016c].The correlation between Atlantic tripole mode index and Atlantic Meridional Mode index is significant at 0.01 level (value of 0.75) for the period 1961–2013 in the observations. This suggests the strong modulation of the Atlantic tripole mode on cluster 3. The SST regions in clusters 4 and 5 are located in the North Pacific, Southwestern Pacific, Indian Ocean, and North Atlantic while the region for Z500 [*Chan et al*., 2001; *Li et al*., 2013] is located in the WNP. It is noted that the spatial correlation maps of SST and Z500 with WNP TC frequency are nearly opposite to one another for clusters 4 and 5 (Figure 14), reflecting different phases of the climate oscillation (e.g., ENSO and AMM). The SST, Z500, and VWS [*Chan et al*., 2001; *Li et al*., 2013] domains of cluster 6 are typical of El Niño years [*Wang and Chan*, 2002; *Camargo and Sobel*, 2005], concurrent with SST regions in the Indian ocean [e.g., *Wang et al*., 2013; *Zhan et al*, 2013] and North Atlantic [*Li et al*., 2013; *Huo et al*., 2015; *Yu et al*., 2015]. TC geneses in cluster 6 (Figure 10) are located southeast of those in cluster 4, consistent with the southeast-northwest pattern of TC genesis during El Niño/La Niña years [*Wang and Chan*, 2002; *Camargo and Sobel*, 2005]. The SST domain of cluster 7 bears strong resemblance to El Niño with significant regions more confined in the Pacific (Figure 14). Therefore, the spatial SST domains of the seven clusters are related to ENSO/PDO, the SST gradient between Southwestern Pacific and warm pool, North Atlantic warming (cooling), the Atlantic tripole mode, the Atlantic Meridional Mode and Indian Ocean SST anomalies, which strongly modulate WNP TC activity based on the literature. Moreover, the domains for Z500 and VWS in the WNP have been widely used to make seasonal forecasting of WNP TCs [e.g., *Chan et al*., 2001; *Li et al*., 2013; *Wang et al*., 2013].

Poisson regression models, which regress the observed WNP TC frequency in each cluster to the predictors, show promising results after leave-one-out cross validation compared to dynamic predictions based on FLOR-FA (Figure 15). The correlation produced by the hybrid models (i.e., combining Poisson regression and FLOR-FA) is higher than those by FLOR-FA alone (Figure 7) in almost all clusters and initialization months. Similarly, the RSME produced by the hybrid models is lower than those by FLOR-FA. For example, the RSME values of clusters 1 and 7 in the hybrid models are smaller than 1 while those in FLOR-FA are larger than 1.5. This indicates that the hybrid model outperforms FLOR-FA in predicting WNP TC frequency in each cluster.

The equations for the hybrid models built by Poisson regression in the January initialization month are shown in Table 3 and those initialized in February months are provided in supporting information Tables S1–S5. The predicted total WNP TC frequency is obtained by summing up predicted TC frequency in each cluster. Figure 13 shows that the approach based on hybrid models can lead to skillful predictions for total WNP TC frequency. The correlations between the observed and predicted WNP TC frequencies in the hybrid model are higher than FLOR-FA when initialized in March, April, May, June, and July (Figures 2 and 16). The correlations in the hybrid model are, however, lower than FLOR-FA initialized in January and February (Figures 2 and 16). The RSME values in the hybrid models are lower than FLOR-FA except when initialized in January and February (Figures 2 and 16). Therefore, the hybrid model, in general, outperforms FLOR-FA in predicting total WNP TC frequency. The predictive skill of WNP TC frequency for different clusters with FLOR-FA initialized in July is better than that initialized in January (Figure 12a). When we build hybrid models for each cluster, the performance of the hybrid models is still influenced by the results with FLOR-FA for different clusters as shown in Figure 12a. After we combine the hybrid models for each cluster, the

Table 4. Landfall Rate Over East Asia for Each of the Seven Clusters (i.e., C1–7) in FLOR-FA and Observations Combined

East Asia	C1	C2	C3	C4	C5	C6	C7
Landfall rate	0.23	0.55	0.82	0.79	0.37	0.25	0.93

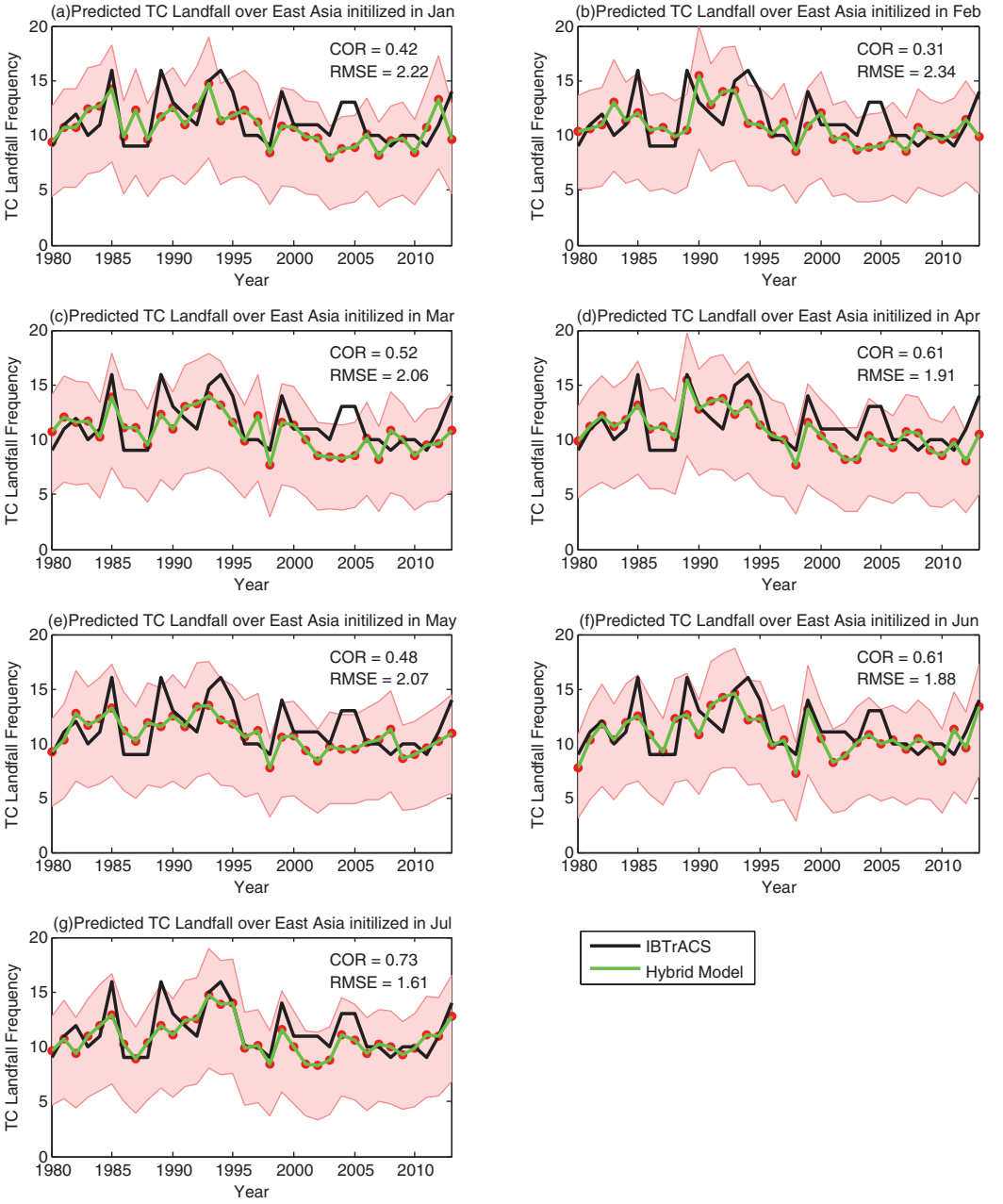

Figure 17. Correlation and RMSE of observed and predicted TC landfall over East Asia produced by the hybrid model by leave-one-out cross validation. The red circles denote the predicted frequency of TC landfall over East Asia in each year using the hybrid model, while the black solid line represents the observations. The pink buffer zones depict the 10% and 90% percentiles of 1000 random sampling of TC landfall frequency over East Asia given μ (the predicted mean landfall TC frequency over East Asia) under Poisson distribution.

predictive skill of the combined hybrid model initialized in January is thus lower than that initialized in July (Figures 2 and 16).

3.2.3. Prediction of TC Landfall Over East Asia

The prediction of landfall frequency over East Asia can be obtained by summing up the landfall frequency over East Asia for the seven clusters. The landfall rate (τ) over East Asia (Figure 1) for each cluster is summarized in Table 4. Cluster 7 has the highest landfall rate (0.93), followed by cluster 3 with a landfall rate of 0.82. Cluster 1 has a landfall rate of 0.23, which is the lowest among the seven clusters (Table 4).

Figure 17 shows the prediction of TC landfall over East Asia initialized from January to July. The correlation coefficients between predicted and observed TC landfall range from 0.31 initialized in February to 0.73

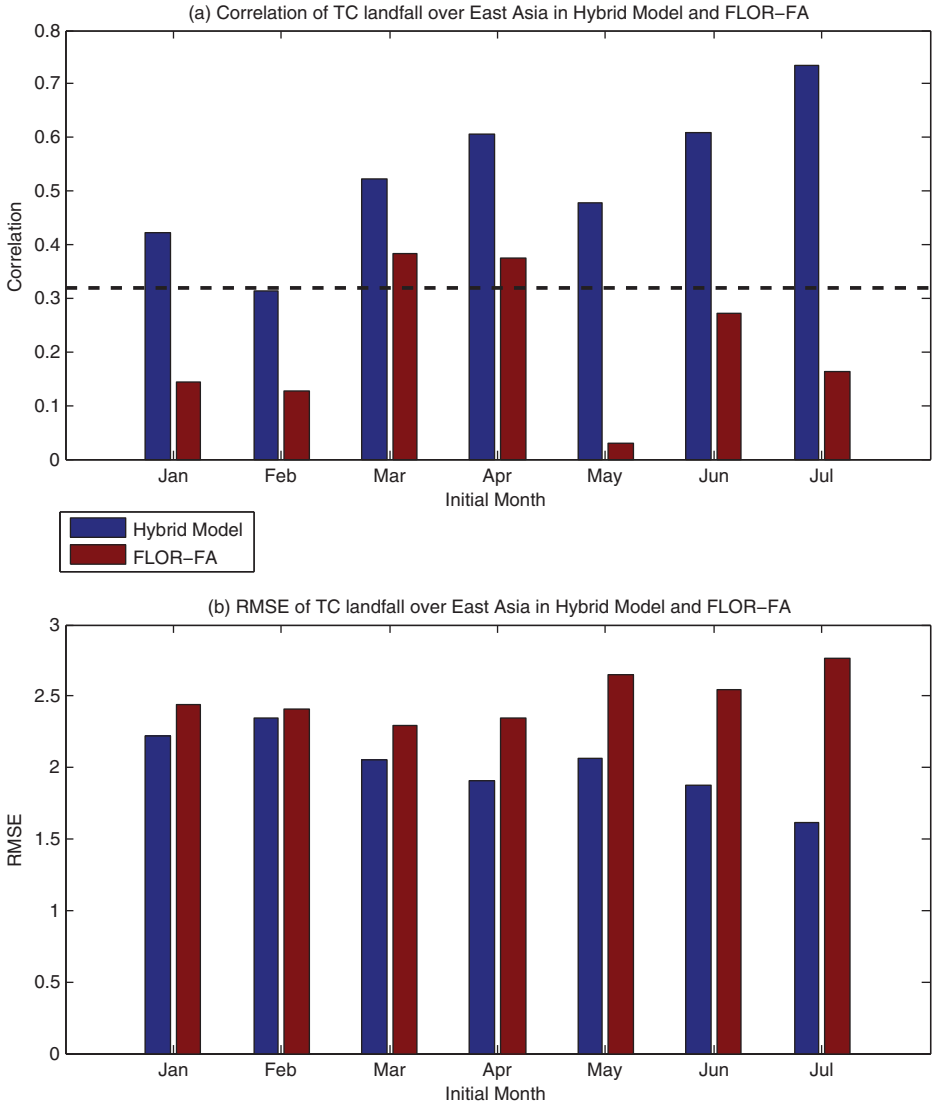

Figure 18. (a) Correlation and (b) RMSE of predicted and observed TC landfall over East Asia using the hybrid model (blue) and FLOR-FA (red) for initialization months January to July. (top) The thick-dashed black line represents the 0.05 level of significance.

initialized in July. The hybrid model performs well in forecasting TC landfall over East Asia in the 1997 and 1998 seasons, especially when initialized in July (Figure 17). The correlations between predicted and observed frequency of TC landfall over East Asia in the hybrid model are statistically significant (the performance of hybrid model initialized in February is a bit lower than the significance level.) and are higher than those in FLOR-FA for all initialization months (Figure 18). Meanwhile, the RMSE values of the TC landfall frequency over East Asia in the hybrid model fluctuate from 1.61 for initialization month July to 2.34 for initialization month February (Figure 18). The predictions initialized in July are encouraging because the RSME in the hybrid model of TC landfall over East Asia is 1.61 while that in FLOR-FA is 2.77 (Figure 16). The RSME values for initialization months from January to July are smaller than those in FLOR-FA (Figure 18).

4. Discussion and Conclusions

Seasonal prediction of TC frequency and landfall has attracted considerable attention from the scientific community. Dynamic models have proven to have high skill in making seasonal predictions of TC frequency, even though systematic biases and uncertainties in these models can affect their forecasting skills. Hybrid models, which are based on the combination of statistical relationships and dynamical models, have

shown promising potential to outperform both statistical and dynamic model predictions [e.g., *Vecchi et al*., 2010, 2013, 2014; *Villarini and Vecchi*, 2013; *Li et al*., 2013]. This study, for the first time, builds a hybrid model for seasonal forecasting of WNP TC frequency and landfall over East Asia by combining cluster analysis results and the retrospective ensemble predictions (hindcasts) of GFDL FLOR-FA with promising performance that outperforms both purely statistical model and dynamic models.

Cluster analysis is taken as the first and one of the most important steps in data processing because it groups the objects (i.e., TCs) exhibiting similarities into the same cluster, and lays the foundation for further data analysis. This study takes advantage of cluster analysis to unravel typical patterns (i.e., clusters) from historical and simulated TC tracks; this information is then used to predict total WNP TC frequency and landfall over East Asia.

This study has applied FMM-based cluster analysis to TC tracks in the WNP produced by FLOR-FA and observations. In total, we identified seven clusters, with three straight-moving and four recurving clusters. Building prediction schemes for each cluster using Poisson regression models allow the prediction of total WNP TC frequency and landfall over East Asia in a rigorous probabilistic framework. The predictions of total WNP TC frequency and TC landfall over East Asia based on cluster analysis results and Poisson regression shows promising capability.

Our research findings can be summarized as follows.

1. Using the FMM-based cluster analysis, seven clusters are identified from the historical and FLOR-FA-predicted TC tracks for the period 1980–2013. FLOR-FA has significant skill in predicting year-to-year variations in the frequency of TCs within certain clusters (i.e., clusters 1 and 5).
2. By building Poisson regression models for each cluster using key predictors (i.e., SST, Z500, and VWS), the predictive skill for almost all the clusters at all initialization months improves with respect to the dynamic predictions. The prediction of total WNP TC frequency made by combining hybrid predictions for each of the seven clusters in the hybrid model shows skill higher than what achieved using the TC frequency directly from FLOR-FA initialized from March to July. However, the hybrid predictions initialized from January to February exhibit lower skill than FLOR-FA.
3. The prediction of TC landfall over East Asia made by combining the landfall rate over East Asia and the hybrid models for TC frequency in each cluster also outperforms FLOR-FA for all start months January through July.

This study has shown that cluster analysis is capable of unraveling hidden and useful patterns within TC tracks, which are highly useful to improve the prediction of total WNP TC frequency and TC landfall over East Asia. *H.-S. Kim et al*. [2012] have also used cluster analysis results to predict TC density in the WNP, though their model is purely statistical. FLOR-FA has some biases in TC density in the WNP, as shown in this study and *Vecchi et al*. [2014]. The biases have been substantially improved in the present control (1990) and SST-nudging experiments with a recently developed 25 km mesh GFDL climate model (HiFLOR) [*Murakami et al*., 2015; *Zhang et al*., 2016b]. Our future work will examine whether HiFLOR produces better seasonal forecasts in the track, genesis, and landfall of WNP TCs within a statistical-dynamical framework.

Acknowledgments
The authors are grateful to the two anonymous reviewers for their insightful comments that led to an improved manuscript. The authors thank Liwei Jia and Baoqiang Xiang for their insightful suggestions that improve an earlier version of this paper. This material is based in part upon work supported by the National Science Foundation under grants AGS-1262091 and AGS-1262099. Tropical cyclone data are obtained from IBTrACS (https://www.ncdc.noaa.gov/ibtracs/). The observed SST data are available from the Met Office Hadley Center (http://www.metoffice.gov.uk/hadobs/hadisst/). The observed large-scale variables are obtained from JRA-55 reanalysis data (http://jra.kishou.go.jp/JRA-55/index_en.html). FLOR B01 data are made available from the NMME project (http://iridl.ldeo.columbia.edu/SOURCES/.Models/.NMME/) and simulations with FLOR-FA are available upon request. The code of FLOR is freely available from GFDL (http://www.gfdl.noaa.gov/cm2-5-and-flor).

References

Au-Yeung, A. M., and J. L. Chan (2012), Potential use of a regional climate model in seasonal tropical cyclone activity predictions in the western North Pacific, *Clim. Dyn.*, *39*, 783–794.

Camargo, S. J., and A. H. Sobel (2005), Western North Pacific tropical cyclone intensity and ENSO, *J. Clim.*, *18*, 2996–3006.

Camargo, S. J., A. W. Robertson, S. J. Gaffney, P. Smyth, and M. Ghil (2007a), Cluster analysis of typhoon tracks. Part II: Large-scale circulation and ENSO, *J. Clim.*, *20*, 3654–3676.

Camargo, S. J., A. W. Robertson, S. J. Gaffney, P. Smyth, and M. Ghil (2007b), Cluster analysis of typhoon tracks. Part I: General properties, *J. Clim.*, *20*, 3635–3653.

Camargo, S. J., A. W. Robertson, A. G. Barnston, and M. Ghil (2008), Clustering of eastern North Pacific tropical cyclone tracks: ENSO and MJO effects, *Geochem. Geophys. Geosyst.*, *9*, Q06V05, doi:10.1029/2007GC001861.

Camp, J., M. Roberts, C. MacLachlan, E. Wallace, L. Hermanson, A. Brookshaw, A. Arribas, and A. A. Scaife (2015), Seasonal forecasting of tropical storms using the Met Office GloSea5 seasonal forecast system, *Q. J. R. Meteorol. Soc.*, *141*, 2206–2219.

Chan, J. C. L. (1995), Prediction of annual tropical cyclone activity over the western North Pacific and the South China Sea, *Int. J. Climatol.*, *15*, 1011–1019.

Chan, J. C. L., J.-E. Shi, and C.-M. Lam (1998), Seasonal forecasting of tropical cyclone activity over the western North Pacific and the South China Sea, *Weather Forecast.*, *13*, 997–1004.

Chan, J. C. L., J. E. Shi, and K. S. Liu (2001), Improvements in the seasonal forecasting of tropical cyclone activity over the western North Pacific, *Weather Forecast.*, *16*, 491–498.
Chang, Y.-S., S. Zhang, A. Rosati, T. Delworth, and W. Stern (2013), An assessment of oceanic variability for 1960–2010 from the GFDL ensemble coupled data assimilation, *Clim. Dyn.*, *40*, 775–803.
Chen, J.-H., and S.-J. Lin (2011), The remarkable predictability of inter-annual variability of Atlantic hurricanes during the past decade, *Geophys. Res. Lett.*, *38*, L11804, doi:10.1029/2011GL047629.
Choi, W., C.-H. Ho, C.-S. Jin, J. Kim, S. Feng, D.-S. R. Park, and J.-K. E. Schemm (2016), Seasonal forecasting of intense tropical cyclones over the North Atlantic and the western North Pacific basins, *Clim. Dyn.*, doi:10.1007/s00382-016-3013-y.
Chu, P.-S., and X. Zhao (2007), A Bayesian regression approach for predicting seasonal tropical cyclone activity over the central North Pacific, *J. Clim.*, *20*, 4002–4013.
Chu, P.-S., X. Zhao, C.-H. Ho, H.-S. Kim, M.-M. Lu, and J.-H. Kim (2010), Bayesian forecasting of seasonal typhoon activity: A track-pattern-oriented categorization approach, *J. Clim.*, *23*, 6654–6668.
Daloz, A. S., et al. (2015), Cluster analysis of downscaled and explicitly simulated north Atlantic tropical cyclone tracks, *J. Clim.*, *28*, 1333–1361.
DelSole, T., and J. Shukla (2009), Artificial skill due to predictor screening, *J. Clim.*, *22*, 331–345.
Delworth, T. L., et al. (2006), GFDL's CM2 global coupled climate models. Part I: Formulation and simulation characteristics, *J. Clim.*, *19*, 643–674.
Delworth, T. L., et al. (2012), Simulated climate and climate change in the GFDL CM2.5 high-resolution coupled climate model, *J. Clim.*, *25*, 2755–2781.
Delworth, T. L., et al. (2015), A link between the hiatus in global warming and North American drought, *J. Clim.*, *28*, 3834–3845.
Deser, C., and M. S. Timlin (1997), Atmosphere–ocean interaction on weekly timescales in the North Atlantic and Pacific, *J. Clim.*, *10*, 393–408.
Du, Y., L. Yang, and S.-P. Xie (2010), Tropical Indian Ocean influence on Northwest Pacific tropical cyclones in summer following strong El Niño*, *J. Clim.*, *24*, 315–322.
Elsner, J. B., and T. H. Jagger (2006), Prediction models for annual US hurricane counts, *J. Clim.*, *19*, 2935–2952.
Elsner, J. B., and C. P. Schmertmann (1993), Improving extended-range seasonal predictions of intense Atlantic hurricane activity, *Weather Forecast.*, *8*, 345–351.
Elsner, J. B., T. H. Jagger, M. Dickinson, and D. Rowe (2008), Improving multiseason forecasts of North Atlantic hurricane activity, *J. Clim.*, *21*, 1209–1219.
Fan, K. (2007), North Pacific sea ice cover, a predictor for the Western North Pacific typhoon frequency?, *Sci. China Ser. D*, *50*, 1251–1257.
Fan, K., and H. Wang (2009), A new approach to forecasting typhoon frequency over the western North Pacific, *Weather Forecast.*, *24*, 974–986.
Farneti, R., T. L. Delworth, A. J. Rosati, S. M. Griffies, and F. Zeng (2010), The role of mesoscale eddies in the rectification of the southern ocean response to climate change, *J. Phys. Oceanogr.*, *40*, 1539–1557.
Gaffney, S., and P. Smyth (1999), Trajectory clustering with mixtures of regression models, In *Proceedings of the Fifth ACM SIGKDD International Conference on Knowledge Discovery and Data Mining*, edited by U. Fayyad, S. Chaudhuri and D. Madigan, Association for Computing Machinery (ACM), N. Y.
Gaffney, S. J. (2004), Probabilistic curve-aligned clustering and prediction with regression mixture models, PhD dissertation, 281p., Univ. of Calif., Irvine.
Gaffney, S. J., A. Robertson, P. Smyth, S. Camargo, and M. Ghil (2007), Probabilistic clustering of extratropical cyclones using regression mixture models, *Clim. Dyn.*, *29*, 423–440.
Goh, A. Z. C., and J. C. L. Chan (2010), An improved statistical scheme for the prediction of tropical cyclones making landfall in South China, *Weather Forecast.*, *25*, 587–593.
Gray, W. M., C. W. Landsea, P. W. Mielke Jr., and K. J. Berry (1993), Predicting Atlantic basin seasonal tropical cyclone activity by 1 August, *Weather Forecast.*, *8*, 73–86.
Holland, G. (1983), Tropical cyclone motion: environmental interaction plus a beta effect, *J. Atmos. Sci.*, *40*, 328–342.
Huang, W.-R., and J. L. Chan (2014), Dynamical downscaling forecasts of Western North Pacific tropical cyclone genesis and landfall, *Clim. Dyn.*, *42*, 2227–2237.
Huo, L., P. Guo, S. N. Hameed, and D. Jin (2015), The role of tropical Atlantic SST anomalies in modulating western North Pacific tropical cyclone genesis, *Geophys. Res. Lett.*, *42*, 2378–2384, doi:10.1002/2015GL063184.
Jia, L., X. et al. (2014), Improved seasonal prediction of temperature and precipitation over land in a high-resolution GFDL Climate Model, *J. Clim.*, *28*, 2044–2062.
Kennedy, J. J., N. A. Rayner, R. O. Smith, D. E. Parker, and M. Saunby (2011), Reassessing biases and other uncertainties in sea surface temperature observations measured in situ since 1850: 2. Biases and homogenization, *J. Geophys. Res.*, *116*, D14104, doi:10.1029/2010JD015220.
Kim, H.-M., and P. J. Webster (2010), Extended-range seasonal hurricane forecasts for the North Atlantic with a hybrid dynamical-statistical model, *Geophys. Res. Lett.*, *37*, L21705, doi:10.1029/2010GL044792.
Kim, H.-M., E. K. M. Chang, and M. Zhang (2014), Statistical-dynamical seasonal forecast for tropical cyclones affecting New York State, *Weather Forecast.*, *30*, 295–307.
Kim, H.-S., J.-H. Kim, C.-H. Ho, and P.-S. Chu (2010), Pattern classification of typhoon tracks using the fuzzy c-means clustering method, *J. Clim.*, *24*, 488–508.
Kim, H.-S., C.-H. Ho, J.-H. Kim, and P.-S. Chu (2012), Track-pattern-based model for seasonal prediction of tropical cyclone activity in the western North Pacific, *J. Clim.*, *25*, 4660–4678.
Kim, J.-H., C.-H. Ho, H.-S. Kim, and W. Choi (2012), 2010 Western north pacific typhoon season: seasonal overview and forecast using a track-pattern-based model, *Weather Forecast.*, *27*, 730–743.
Klotzbach, P. J. (2007), Revised prediction of seasonal Atlantic basin tropical cyclone activity from 1 August, *Weather Forecast.*, *22*, 937–949.
Knaff, J. A., C. R. Sampson, and M. DeMaria (2005), An operational statistical typhoon intensity prediction scheme for the western North Pacific, *Weather Forecast.*, *20*, 688–699.
Knapp, K. R., M. C. Kruk, D. H. Levinson, H. J. Diamond, and C. J. Neumann (2010), The international best track archive for climate stewardship (IBTrACS), *Bull. Am. Meteorol. Soc.*, *91*, 363–376.
Kwon, H. J., W.-J. Lee, S.-H. Won, and E.-J. Cha (2007), Statistical ensemble prediction of the tropical cyclone activity over the western North Pacific, *Geophys. Res. Lett.*, *34*, L24805, doi:10.1029/2007GL032308.

Krishnamurthy, L., G. A. Vecchi, R. Msadek, H. Murakami, A. T. Wittenberg, and F. Zeng (2016), Impact of strong ENSO on regional tropical cyclone activity in a high-resolution climate model in the North Pacific and North Atlantic Oceans, *J. Clim.*, *29*, 2375–2394.
Landsea, C. W., G. D. Bell, W. M. Gray, and S. B. Goldenberg (1998), The extremely active 1995 Atlantic hurricane season: Environmental conditions and verification of seasonal forecasts, *Mon. Weather Rev.*, *126*, 1174–1193.
LaRow, T. E. (2013), The impact of SST bias correction on north Atlantic hurricane retrospective forecasts, *Mon. Weather Rev.*, *141*, 490–498.
Li, X., S. Yang, H. Wang, X. Jia, and A. Kumar (2013), A dynamical-statistical forecast model for the annual frequency of western Pacific tropical cyclones based on the NCEP Climate Forecast System version 2, *J. Geophys. Res. Atmos.*, *118*, 12,061–12,074, doi:10.1002/2013JD020708.
Liu, K. S., and J. C. L. Chan (2003), Climatological characteristics and seasonal forecasting of tropical cyclones making landfall along the South China Coast, *Mon. Weather Rev.*, *131*, 1650–1662.
Lu, M.-M., P.-S. Chu, and Y.-C. Lin (2010), Seasonal prediction of tropical cyclone activity near Taiwan using the Bayesian multivariate regression method, *Weather Forecast.*, *25*, 1780–1795.
Marks, F. D., and L. K. Shay (1998), Landfalling tropical cyclones: Forecast problems and associated research opportunities, *Bull. Am. Meteorol. Soc.*, *79*, 305–323.
McLachlan, G., and T. Krishnan (1997), *The EM Algorithm and Extensions*, John Wiley, N. Y.
Msadek, R., G. A. Vecchi, M. Winton, and R. G. Gudgel (2014a), Importance of initial conditions in seasonal predictions of Arctic sea ice extent, *Geophys. Res. Lett.*, *41*, 5208–5215, doi:10.1002/2014GL060799.
Msadek, R., et al. (2014b), Predicting a decadal shift in North Atlantic climate variability using the GFDL forecast system, *J. Clim.*, *27*, 6472–6496.
Murakami, H., et al. (2015), Simulation and prediction of Category 4 and 5 hurricanes in the high-resolution GFDL HiFLOR coupled climate model, *J. Clim.*, *28*, 9058–9079.
Murakami, H., G. Villarini, G. A. Vecchi, and W. Zhang (2016), Statistical-dynamical seasonal forecast of North Atlantic and U.S. Landfalling tropical cyclones using the high-resolution GFDL FLOR coupled model, *Mon. Weather Rev.*, doi:10.1175/MWR-D-15-0308.1, in press.
Nicholls, N. (1979), A possible method for predicting seasonal tropical cyclone activity in the Australian region, *Mon. Weather Rev.*, *107*, 1221–1224.
Pielke, R. (1997), *Hurricanes: Their Nature and Impacts on Society*, John Wiley, Chichester, England.
Pielke, R., Jr., J. Gratz, C. Landsea, D. Collins, M. Saunders, and R. Musulin (2008), Normalized hurricane damage in the United States: 1900–2005, *Nat. Hazards Rev.*, *9*, 29–42.
Powell, M. D., and S. H. Houston (1998), Surface wind fields of 1995 Hurricanes Erin, Opal, Luis, Marilyn, and Roxanne at landfall, *Mon. Weather Rev.*, *126*, 1259–1273.
Ramsay, H., S. Camargo, and D. Kim (2011), Cluster analysis of tropical cyclone tracks in the Southern Hemisphere, *Clim. Dyn.*, *39*, 897–917.
Smith, D. M., R. Eade, N. J. Dunstone, D. Fereday, J. M. Murphy, H. Pohlmann, and A. A. Scaife, 2010: Skilful multi-year predictions of Atlantic hurricane frequency, *Nat. Geosci.*, *3*, 846–849.
Sun, J., and J. Ahn (2011), A GCM-based forecasting model for the landfall of tropical cyclones in China, *Adv. Atmos. Sci.*, *28*, 1049–1055.
Sun, J., and H. Chen (2011), Predictability of western North Pacific typhoon activity and its factors using DEMETER coupled models, *Chin. Sci. Bull.*, *56*, 3474–3479.
Tan, P.-V., T. T. Long, B.-H. Hai, and K. Chanh (2015), Seasonal forecasting of tropical cyclone activity in the coastal region of Vietnam using RegCM4.2, *Clim. Res.*, *62*, 115–129.
Vecchi, G. A., and G. Villarini (2014), Next season's hurricanes, *Science*, *343*(6171), 618–619.
Vecchi, G. A., M. Zhao, H. Wang, G. Villarini, A. Rosati, A. Kumar, I. M. Held, and R. Gudgel (2011), Statistical-dynamical predictions of seasonal north Atlantic hurricane activity, *Mon. Weather Rev.*, *139*, 1070–1082.
Vecchi, G. A., et al. (2013), Multiyear predictions of North Atlantic hurricane frequency: Promise and limitations, *J. Clim.*, *26*, 5337–5357.
Vecchi, G. A., et al. (2014), On the seasonal forecasting of regional tropical cyclone activity, *J. Clim.*, *27*, 7994–8016.
Villarini, G., and G. A. Vecchi (2013), Multiseason lead forecast of the north Atlantic power dissipation index (PDI) and accumulated cyclone energy (ACE), *J. Clim.*, *26*, 3631–3643.
Villarini, G., G. A. Vecchi, and J. A. Smith (2010), Modeling of the dependence of tropical storm counts in the North Atlantic Basin on climate indices, *Mon. Weather Rev.*, *138*(7), 2681–2705.
Villarini, G., G. A. Vecchi, and J. A. Smith (2012), U.S. Landfalling and North Atlantic hurricanes: Statistical modeling of their frequencies and ratios, *Mon. Weather Rev.*, *140*, 44–65.
Vitart, F., M. R. Huddleston, M. Déqué, D. Peake, T. N. Palmer, T. N. Stockdale, M. K. Davey, S. Ineson, and A. Weisheimer (2007), Dynamically-based seasonal forecasts of Atlantic tropical storm activity issued in June by EUROSIP, *Geophys. Res. Lett.*, *34*, L16815, doi:10.1029/2007GL030740.
Wang, B. and J. C. L. Chan (2002), How strong ENSO events affect tropical storm activity over the Western North Pacific, *J. Clim.*, *15*, 1643–1658.
Wang, B., B. Xiang, and J.-Y. Lee (2013), Subtropical high predictability establishes a promising way for monsoon and tropical storm predictions, *Proc. Natl. Acad. Sci. U. S. A.*, *110*, 2718–2722.
Wang, H., J.-K. E. Schemm, A. Kumar, W. Wang, L. Long, M. Chelliah, G. D. Bell, and P. Peng (2009), A statistical forecast model for Atlantic seasonal hurricane activity based on the NCEP dynamical seasonal forecast, *J. Clim.*, *22*, 4481–4500.
Wilks, D. S. (2011), *Statistical Methods in the Atmospheric Sciences*, vol. 100, Academic, Burlington, Mass.
Wu, M., W. Chang, and W. Leung (2004), Impacts of El Niño-Southern Oscillation events on tropical cyclone landfalling activity in the western North Pacific, *J. Clim.*, *17*, 1419–1428.
Yang, X., et al. (2012), A predictable AMO-like pattern in the GFDL fully coupled ensemble initialization and decadal forecasting system, *J. Clim.*, *26*, 650–661.
Yang, X., et al. (2015), Seasonal predictability of extratropical storm tracks in GFDL's high-resolution climate prediction model, *J. Clim.*, *28*, 3592–3611.
Yu, J., T. Li, Z. Tan, and Z. Zhu (2015), Effects of tropical North Atlantic SST on tropical cyclone genesis in the western North Pacific, *Clim. Dyn.*, *3*, 865–877.
Zhan, R., Y. Wang, and X. Lei (2010), Contributions of ENSO and East Indian Ocean SSTA to the Interannual Variability of Northwest Pacific Tropical Cyclone Frequency, *J. Clim.*, *24*, 509–521.
Zhan, R., Y. Wang, and M. Wen (2013), The SST Gradient between the southwestern Pacific and the western Pacific Warm Pool: A New factor controlling the northwestern Pacific tropical cyclone genesis frequency, *J. Clim.*, *26*, 2408–2415.
Zhang, Q., Q. Liu, and L. Wu (2009), Tropical cyclone damages in China 1983-2006, *Bull. Am. Meteorol. Soc.*, *90*, 489–495.

Zhang, S., and A. Rosati (2010), An inflated ensemble filter for ocean data assimilation with a biased coupled GCM, *Mon. Weather Rev.*, *138*, 3905–3931.

Zhang, S., M. J. Harrison, A. Rosati, and A. Wittenberg (2007), System design and evaluation of coupled ensemble data assimilation for global oceanic climate studies, *Mon. Weather Rev.*, *135*, 3541–3564.

Zhang, W., H. F. Graf, Y. Leung, and M. Herzog (2012), Different El Niño types and tropical cyclone landfall in East Asia, *J. Clim.*, *25*, 6510–6523.

Zhang, W., Y. Leung, and J. C. L. Chan (2013a), The analysis of tropical cyclone tracks in the western North Pacific through data mining. Part I: Tropical cyclone recurvature, *J. Appl. Meteorol. Climatol.*, *52*, 1394–1416.

Zhang, W., Y. Leung, and J. C. L. Chan (2013b), The analysis of tropical cyclone tracks in the western North Pacific through data mining. Part II: Tropical cyclone landfall, *J. Appl. Meteorol. Climatol.*, *52*, 1417–1432.

Zhang, W., Y. Leung, and Y. Wang (2013c), Cluster analysis of post-landfall tracks of landfalling tropical cyclones over China, *Clim. Dyn.*, *40*, 1237–1255.

Zhang, W., S. Gao, B. Chen, and K. Cao (2013d), The application of decision tree to intensity change classification of tropical cyclones in western North Pacific, *Geophys. Res. Lett.*, *40*, 1883–1887, doi:10.1002/grl.50280.

Zhang, W., Y. Leung, and J. Min (2013e), North Pacific Gyre oscillation and the occurrence of western North Pacific tropical cyclones, *Geophys. Res. Lett.*, *40*, 5205–5211, doi:10.1002/grl.50955.

Zhang, W., B. Fu, M. S. Peng, and T. Li (2015), Discriminating developing versus nondeveloping tropical disturbances in the western North Pacific through decision tree analysis, *Weather Forecast.*, *30*, 446–454.

Zhang W., G. A. Vecchi, H. Murakami, G. Villarini, and L. Jia (2016a), The Pacific meridional mode and the occurrence of tropical cyclones in the western North Pacific, *J. Clim.*, *29*, 381–398.

Zhang, W., et al. (2016b), Improved simulation of tropical cyclone responses to ENSO in the western North Pacific in the high-resolution GFDL HiFLOR coupled climate model, *J. Clim.*, *29*, 1391–1415.

Zhang W., G. A. Vecchi, H. Murakami, G. Villarini, T Rosati, L. Jia (2016c), Modulation of Western North Pacific Tropical Cyclone Activity by the Atlantic Meridional Mode, *Clim. Dyn.*, doi:10.1007/s00382-016-3099-2.

Zhao, M., I. M. Held, and G. A. Vecchi (2010), Retrospective forecasts of the hurricane season using a global atmospheric model assuming persistence of SST anomalies, *Mon. Weather Rev.*, *138*, 3858–3868.